Am J Transl Res 2023;15(8):5007-5034
www.ajtr.org /ISSN:1943-8141/AJTR0150921

Original Article

C18ORF54 promotes immune infiltration and poor prognosis as a potential biomarker for hepatocellular carcinoma

Yuyu Ma[1*], Dong Yan[2*], Fengming Tian[1*], Wen Song[3], Ruocheng Sha[1], Xiaoqian Shang[1], Jie Lv[1], Naifeisha Maimaiti[1], Panpan Kong[2], Xiumin Ma[1]

[1]State Key Laboratory of Pathogenesis, Prevention and Treatment of High Incidence Diseases in Central Asia, Clinical Laboratory Center, Tumor Hospital Affiliated to Xinjiang Medical University, Urumqi 830011, Xinjiang, P. R. China; [2]The First Ward of Hepatobiliary and Pancreatic Surgery, Tumor Hospital Affiliated to Xinjiang Medical University, Urumqi 830011, Xinjiang, P. R. China; [3]Clinical Laboratory Center, Hospital of Traditional Chinese Medicine Affiliated to Xinjiang Medical University, Urumqi 830099, Xinjiang, P. R. China. [*]Equal contributors.

Received April 26, 2023; Accepted July 26, 2023; Epub August 15, 2023; Published August 30, 2023

Abstract: Objective: The morbidity of hepatocellular carcinoma (HCC) is increasing annually. The aim of this study is to investigate the molecular mechanisms of upregulated genes in HCC using bioinformatic methods, so as to identify new potential biological markers. Methods: The Gene Expression Omnibus database (GEO database) was mined for HCC datasets, which were screened for hub genes and subjected to (Gene Ontology) GO and (Kyoto Encyclopedia of Genes and Genomes) KEGG enrichment analysis. The hub genes were analyzed in terms of Receiver Operating Characteristic (ROC) and methylation levels. Validation of hub genes was completed through basic pathological alterations based on the protein and gene expression level of hub genes. The correlation of genes with immune infiltration in HCC was analyzed based on the database Timer 2.0, and the prognosis as well as survival of hub genes in HCC was analyzed using R studio software. Finally, we performed a gene combination drug analysis on the potential therapeutic targets in HCC. Results: Expression-up-regulated genes were screened via differential analysis, which were mainly enriched in cell cycles and DNA replication pathways. Five hub genes, BRCA1 associated RING domain 1 (BARD1), Mismatch Repair Protein (MSH2), Recombinant H2A Histone Family, Member X (H2AFX), Recombinant H2A Histone Family, Member z (H2AFZ) and Chromosome 18 Open Reading Frame 54 (C18orf54) were identified using a Protein-Protein Interaction Networks (PPI). After a comprehensive analysis of ROC curves and methylation gene mutation sites, C18orf54 was localized followed by basic experiments, so as to verify the C18orf54 upregulated in HCC. Based on the online database Timer 2.0, the immune infiltration of C18orf54 gene in HCC was analyzed, which was found to be negatively correlated with $CD4^+$ T cells and macrophages in HCC, meanwhile a further refinement of the immune checkpoint correlation analysis revealed that C18orf54 was mainly correlated with Hepatitis A virus cellular receptor 2 (HAVCR2), T cell immunoreceptor with Ig and ITIM domains (TIGIT) and Cytotoxic T lymphocyte associate protein-4 (CTLA4). The prognosis and survival of patients with HCC expressing C18orf54 were also analyzed, and it was found that such patients had a higher incidence of adjacent liver tissue inflammation, a higher child-Pugh grade score and a higher rate of residual tumor recurrence. Similarly, the prognosis was worse in the subset of patients with C18orf54. Finally, we performed a combined genetic analysis, which suggested that cyclosporine, quercetin, testosterone and calcitriol might be effective in reducing C18orf54 mRNA expression. Conclusion: C18orf54 is involved in the immune infiltration and promotes the poor prognosis of HCC, which could be a candidate biomarker for HCC.

Keywords: Hepatocellular carcinoma, C18orf54, immune infiltration, prognosis

Introduction

The morbidity of hepatocellular carcinoma (HCC) is increasing and has become the second leading cause of cancer death worldwide [1-3]. Currently, the main treatment options for HCC include immunotherapy and multi-tyrosine kinase inhibitors [4-7]. However, treatment outcomes are unsatisfactory due to the drug resistance of HCC cells [8-10], and the high mortality

of HCC shows no marked improvement due to the lack of accurate early diagnosis [11]. Therefore, uncovering the molecular mechanisms of HCC will help improve the accuracy of early diagnosis and develop effective therapeutic targets for hepatocellular carcinoma. Currently, methemoglobin and des-γ-carboxyplasminogen have been widely used as prognostic biomarkers for detecting HCC. However, their sensitivities are far from satisfactory [12, 13]. Therefore, there is an urgent need to find new therapeutic biomarkers for HCC. Several studies have shown that bioinformatics analysis could be used to identify valuable functional genes [14-16]. The Gene Expression Omnibus database (GEO database) was retrieved for HCC datasets and a total of 192 up-regulated genes was screened, while five hub gene were identified by Cytoscape software, namely BRCA1 associated RING domain 1 (BARD1), Mismatch Repair Protein (MSH2), Recombinant H2A Histone Family, Member X (H2AFX), Recombinant H2A Histone Family, Member z (H2AFZ) and Chromosome 18 Open Reading Frame 54 (C18orf54), and that upregulation of BARD1 could promote HCC progression by targeting Akt signaling [17]. These findings provide MSH2 SNP, rs2303428, as a novel prognostic biomarker for HCC patients [18]. It has also been suggested that the H2AFX gene may be a potential poor prognostic biomarker in HCC and may be involved in the infiltration of HCC immune cells [19]. A comprehensive analysis has also now shown the potential value of H2AFZ as a novel prognostic indicator and its association with immune infiltration in HCC, laying the foundation for future studies in HCC investigation and intervention [20]. C18orf54 is a protein-coding gene predicted to act upstream of or within the proliferation of cell populations, which, located in the extracellular region, may play a role in cell proliferation. Diseases associated with C18orf54 include lung adenoma and adenoma, but the mechanism through which C18orf54 accelerates HCC progression is unclear, nor has its role in tumor immunity been determined. In this study, we propose to explore the immune infiltration, prognosis and drug action targets of HCC, aiming to explore the potential bioinformatic functions and gene regulatory network of C18orf54 in HCC, meanwhile providing potential therapeutic targets for the treatment and prognosis of HCC.

Materials and methods

Microarray data source

"Hepatocellular carcinoma" was used as a keyword to search the Gene Expression Omnibus (http://www.ncbi.nlm.nih.gov/geo) public database. We downloaded the microarray expression profiling dataset GSE84402 stored by Qin W, Jin H, Wang H [21] in 2017. This dataset was based on GPL570 [HG-U133_Plus_2] Affymetrix Human Genome U133 Plus 2.0 Array. The dataset collected a total RNA of 7 pairs of hepatocellular carcinoma tissues and corresponding non-cancerous tissues, including 7 hepatocellular carcinoma tissues and 7 healthy controls. We also downloaded the microarray expression profiling dataset GSE-101685 saved by Sen-Yung H in 2019. This dataset was also based on GPL570 [HGU133_Plus_2] Affymetrix Human Genome U133 Plus 2.0 Array. This dataset selected 8 normal tissues and 24 hepatocellular carcinoma patients at T1, T3a, and T3b stages for RNA extraction and displayed the gene expression profile. In addition, we downloaded the microarray expression profiling dataset GSE62232 saved by Zucman-Rossi J, Imbeaud S, Couchy G [22] in 2014. This dataset, based on GPL570 [HG-U133_Plus_2] Affymetrix Human Genome U133 Plus 2.0 Array, collected liver tumors from 81 hepatocellular carcinoma patients. Finally, we downloaded the microarray expression profiling dataset GSE112790 saved by Shimada S, Mogushi K, Akiyama Y, Furuyama T etc. [23] in 2019. This dataset was based on GPL570 [HG-U133_Plus_2] Affymetrix Human Genome U133 Plus 2.0 Array. This dataset involved 183 patients who underwent curative liver resection for liver cancer at Tokyo Medical and Dental University Hospital from 2006 to 2013. Fifteen adjacent liver tissues obtained from colorectal cancer metastasis patients who had never received chemotherapy served as controls. Because this dataset and the annotation file were downloaded from a public database, patient consent and ethical committee approval were not required. The clean data from the above databases were exported using R Studio, and volcano plots were exported according to the differential analysis (filtering criteria: volcano plot threshold is |logFC| >1 & p-value < 0.05). After the genes from the above databases were processed, the up-regulated

genes in hepatocellular carcinoma were screened according to logFC >1, P < 0.05; the down-regulated genes in hepatocellular carcinoma were screened according to logFC < -1, P < 0.05.

Identifying differentially expressed up-regulated genes in hepatocellular carcinoma

We normalized and preprocessed the data. RStudio software (v4.0.3) was used for standardization preprocessing and ID conversion of the data. The 'limma' package was used to identify differently expressed genes between hepatocellular carcinoma and control specimens, with an adjusted *p*-value < 0.05 and |log2 (fold change)| >1 as the screening criteria. Genes that met these conditions were included in the differently expressed genes. The 'ggplot2' package and 'Pheatmap' package were used to visualize the images.

Finally, up-regulated differently expressed genes in hepatocellular carcinoma were selected from each of the four databases. The common genes from these four databases were identified using an online Venn diagram construction site (https://bioinfogp.cnb.csic.es/tools/venny/index.html). All these common genes were included in the further analysis.

Enrichment analysis

The Database for Annotation, Visualization and Integrated Discovery (DAVID) (https://david.ncifcrf.gov/), first released in 2003, can help users extract comprehensive biological annotation information and gene ID conversion from large-scale gene or protein lists. This data is mainly used to identify gene function differences, pathway enrichment analysis, and cluster analysis. This study mainly used it for gene ontology (GO) biological process (BP)/cellular component (CC)/molecular function (MF) and Kyoto Encyclopedia of Genes and Genomes (KEGG) enrichment analysis (information sourced from the official website).

Differentially expressed genes were input into the DAVID database for GO BP/CC/MF enrichment analysis. Specifically, the *p*-values of the enrichment results are represented by color, and the gene count is represented by the size of the bubbles.

Next, we carried out a detailed analysis of the basic functions of the genes. The functions of the genes are divided into three categories: Biological Process, Cellular Component, and Molecular Function. Using the 'clusterProfiler' package, we can obtain the association of target genes at the CC, MF, and BP levels, as well as the visualization of related graphics.

Construction of PPI network and identification of hub genes

The Functional Protein Association Networks (String) database (http://string-db.org) is currently updated to version 11.5, storing information on 14,094 species, 67,592,464 proteins, and 20,052,394,041 interactions. It can be used to retrieve a database of interactions between known proteins and predicted proteins (information sourced from the official website).

The STRING online analysis database performs related analyses at the protein interaction level: statistical analysis and visualization are both carried out in R version 3.6.3. We put the differently expressed genes we screened into the STRING database for protein interaction analysis.

Then the STRING data was imported into Cytoscape. Cytoscape is software for open-source network visualization and analysis. It provides basic functionality for layout and querying networks, and forms visualized networks based on basic data combination. Originating from systems biology, Cytoscape integrates molecular interaction networks, high-throughput gene expression data, and other molecular state information. It is now widely used for large-scale protein-protein interaction and genetic interaction analysis.

Finally, the hub genes in the PPI protein interaction network diagram were identified using MCODE (v2.0.0).

UALCAN analysis

The University of Alabama at Birmingham Cancer data analysis Portal (UALCAN) (http://UALCAN.path.uab.edu) provides potential gene relative transcription expression between normal and tumor samples, as well as the association of relative clinical parameters with tran-

scription expression. In our research, we used the UALCAN database to explore the mRNA expression between hepatocellular carcinoma tissues and normal tissues. Data analysis was conducted with t-tests, and a *p*-value less than 0.05 was considered statistically significant.

Hub gene ROC curve drawing

Data was sourced from the Cancer Genome Atlas (TCGA) (https://portal.gdc.cancer.gov/) LIHC (liver hepatocellular carcinoma) project level 3 HT Seq-FPKM formatted RNA seq data. Data process RStudio software (v3.6.3) was used for statistical analysis and visualization processing. The pROC package (1.17.0.1) and ggplot2 package (3.3.3) were used to visualize the ROC curve for C18orf54 in patients with hepatocellular carcinoma.

Hub gene methylation analysis

Data was sourced from TCGA (https://portal.gdc.cancer.gov/) LIHC (liver hepatocellular carcinoma) project, level 3 HTSeq-FPKM formatted RNAseq data, and Illumina Human Methylation 450 methylation data. R (version 3.6.3) and the R package, mainly ggplot2 (version 3.3.3) (used for visualization), were used. Data transformation: FPKM (Fragments Per Kilobase per Million) formatted RNAseq data was transformed into TPM (Transcripts Per Million reads) format and log2 transformed. Data filtering: removal of control/normal (not all projects have control/normal) + removal of duplicate samples. Finally, t-tests were conducted for statistical analysis, and a *p*-value less than 0.05 was considered statistically significant.

UCSC genome browser

The University of California Santa Cruz (UCSC) (http://genome.ucsc.edu/) is a significant biological database created and maintained by the University of California, Santa Cruz (UCSC) since 2000, and is widely used in genome research. It contains a wealth of genomic data for a variety of vertebrates and model organisms, including gene annotation information (ENCODE), inter-genomic comparison information, repeat sequences, homologous sequences, reference sequences (mRNA, EST), phenotypes, expression spectra, regulatory information, conservations, mutations, repeat regions, and a series of other information for public viewing, analysis, and free downloading. In this study, this database was primarily used for the thorough visualization of the sequence location of the C18orf54 gene.

cBioPortal

The cBioPortal database (http://cbioportal.org) was developed in honor of the Memorial Sloan-Kettering Cancer Center (MSKCC) in the United States, and it is specifically designed to address the data integration issues brought about by large cancer genome projects. Its data come from multiple platforms, including The Cancer Genome Atlas, the International Cancer Genome Consortium (ICGC), the Integrative Genomics Viewer (IGV), the University of California Santa Cruz (UCSC), Oncomine, and others. cBioPortal studies an extremely rich variety of gene types, including somatic mutations, DNA copy number changes, mRNA and microRNA expressions, DNA methylation, protein abundance, and phosphoprotein abundance, all of which are available for public download.

Users can view the gene alteration patterns of various samples in cancer research, relevant genomic/spectrographic changes, and further compare the frequency of gene alterations in different cancer studies. This tool is used for interactive exploration of multiple cancer genomics data sets and clinically relevant research. The database also supports pathway, survival analysis, and exclusivity analysis between genomic changes. At the same time, it visualizes gene data and clinical data (source from the official website).

In this study, its data visualization processing function is mainly utilized. In the cBioPortal database, we input the final determined C18orf54 gene to visualize its structural domain (Supplement Figure 1A).

Human Protein Atlas

The Human Protein Atlas (HPA) database is based on proteomics, transcriptomics, and systems biology data, which can be used to create atlases of tissues, cells, and organs (https://www.proteinatlas.org). In our study, we used the HPA database to visualize the RNA expression levels of C18orf54 in normal tissues, transformed into nTPM.

Single Cell Expression Atlas

The Single Cell Expression Atlas supports single-cell transcriptomics research. The Atlas uses ontology identifiers to annotate publicly available single-cell RNA-Seq experiments and reanalyzes them using the standardization pipeline provided by the RNA-Seq analysis toolkit IRAP. It also supports the search for gene expression within and between studies (https://www.ebi.ac.uk/gxa/sc/home). In our study, we used it to analyze the single cells of normal testis tissue and normal liver tissue for C18orf54. After transforming the data into t-SNE, we visualized it.

Liver cancer samples

From May to September 2022, liver cancer patients who underwent surgery at the Third Affiliated Hospital of Xinjiang Medical University were selected. Tumor tissues and margin tissues far from the tumor site were surgically removed from 7 patients. In addition, the clinical medical records of these 7 liver cancer patients were collected. This study was approved by the Ethics Committee of the Third Affiliated Hospital of Xinjiang Medical University and conducted according to the Declaration of Helsinki. All patients provided informed consent and agreed to participate in the research. HCC tissues were immediately preserved in situ at -80°C for RNA and protein extraction.

The specific inclusion and exclusion criteria are as follows: Inclusion criteria: (1) Postoperative pathology confirmed liver cancer with a clear pathological diagnosis. Clinical pathological staging was based on the 7th edition of the TNM staging system developed by the International Union Against Cancer and the American Cancer Society. (2) The patient was diagnosed with liver cancer for the first time, with no distant metastasis. (3) The patient did not receive any treatment before surgery. (4) Complete follow-up information. (5) No other serious malignant diseases. (6) Clinical, pathological, and surgical data are available. Exclusion criteria: (1) Individuals who cannot communicate normally. (2) Patients with organ dysfunction of the heart, brain, lung, and kidney. (3) Patients who were diagnosed with liver cancer for the first time and had distant metastases. (4) Patients with incomplete clinical and pathological data. (5) Patients with systemic diseases. (6) Patients with autoimmune dysfunction.

H&E staining

Paraffin sections were deparaffinized with xylene and ethanol, followed by hematoxylin-eosin (H&E) staining, ethanol dehydration, xylene transparency, and neutral resin fixation. The liver tissue sections were then placed under an Olympus optical microscope. Under 10× magnification, the general staining results were observed. Under 20× magnification, five different fields of view with pathological changes were randomly selected. They were then enlarged to 40× magnification for detailed observation of pathological changes, and five different fields of view with obvious pathological change features were randomly selected. Hematoxylin, an alkaline solution, stains the basophilic cell nucleus blue. Eosin, as an acidic dye, combines with the positive cations of amino acids in proteins to stain the cytoplasm, so the cytoplasm and eosinophilic granules are stained different degrees of red or pink. Observation, photography, and pathological scoring were performed under an optical microscope.

IHC immunohistochemistry

After dewaxing the tissue sections, antigen repair was performed with citrate buffer for 15 min, endogenous peroxidase blocking agent was kept in the dark at room temperature for 10 min, and goat serum was sealed for 20 min. They were then incubated with anti-C18orf54 (1:500, Shanghai House China) overnight in a 4°C refrigerator. The next day, the sections were incubated with secondary antibodies at 37°C for 90 min, followed by DAB staining, differentiation, and return blue, dehydration, and transparency, drying and sealing. The stained liver tissue sections were placed under an Olympus optical microscope. The general staining results were observed under 10× magnification, and five different fields of view were randomly selected under 20× magnification. Under 40× magnification, the positive expression areas were determined and five different fields of view were randomly selected. The pictures were put into Image J software to calculate the brown positive area and the negative area without staining changes in each stained picture.

Finally, statistical analysis of the results was performed using SPSS 21.0 software.

IF immunofluorescence co-localization

After dewaxing the tissue sections, antigen repair was performed with citrate buffer for 15 min, endogenous peroxidase blocking agent was kept in the dark at room temperature for 10 min, and goat serum was sealed for 20 min. They were then incubated with anti-C18orf54 (1:500, Shanghai House China) overnight in a 4°C refrigerator. The next day, they were incubated with a secondary fluorescent antibody for 1 hour and then incubated with 4,6-diamino-2-phenylindole (DAPI) in the sealing solution for 5 minutes and incubated in a humid chamber at 37°C for 30 minutes. The IF signal was observed under a fluorescence microscope. The liver tissue sections finished with immunofluorescence staining were placed under a confocal fluorescence microscope. A professional lab teacher operated the microscope, and five different fields of view were randomly selected under 20× magnification. The pictures were put into Image J software to calculate the positive cell area and the negative area without staining changes in each stained picture. Finally, statistical analysis of the results was performed using SPSS 21.0 software.

Western blot

Total proteins were separated from hepatocellular carcinoma tissues (tumor tissues and paired normal adjacent tissues) and cell lines with protein extraction buffer (RIPA lysis buffer). A total of 30 μg/hole proteins were run on 12% SDS-PAGE. The membrane was incubated with 5% skim milk powder at room temperature for 1 hour. It was then incubated at 4°C with anti-C18orf54 antibody (1:1000, Shanghai House, Cat. Number: HK7516) and anti-GAPDH antibody (1:5000, ab8245, Abcam, USA). Then, the membrane was incubated with the appropriate secondary antibody. The bands were observed by enhanced chemiluminescence (EMD Millipore). GAPDH was used as a loading control. The bands were placed in a chemiluminescence apparatus, an appropriate amount of developer was added for exposure, and the results were recorded and photographed for preservation. The gray values of the bands were later analyzed using Image Lab software.

Q-RTPCR real-time quantitative fluorescent PCR

Total RNA for quantitative real-time PCR (qRT-PCR) was extracted from HCC tumor tissues, paired normal adjacent tissues, and cell lines using TRIzol reagent (TaKaRa, Japan). The PrimeScript RT reagent kit (Reagent Number: RR047A) was used to convert RNA into cDNA under the following thermocycling conditions: processing at 42°C for 2 minutes, followed by infinite cycles at 4°C. A Real-Time PCR reaction was performed, with a two-step PCR amplification program: first step at 95°C for 30 seconds for pre-denaturation, and second step of 40 PCR cycles at 95°C for 5 seconds, followed by a reaction at 60°C for 30~34 seconds. The qRT-PCR primer designs were as follows: C18orf54, forward: 5'-GCACTTTTGCCATCAGCTTATTT-3', reverse: 5'-CTCGGTGAATATCTCCCGTCTTTG-3'. GAPDH, forward: 5'-GTC GGT GTG AAC GGA TTT G-3', reverse: 5'-TCC CAT TCT CAG CCT TGA C-3'.

The 2-ΔCq method was used and normalized to the internal reference gene GAPDH. After the reaction ended, the reaction system was taken out promptly to avoid contamination, and the dissolution curve of each indicator was checked promptly. The Ct values of all samples were recorded, and the expression of the target gene was quantitatively analyzed using the 2-ΔΔCt method.

TIMER2.0 analysis

TIMER2.0 is a comprehensive online server resource providing systematic analyses of immune infiltration across various types of cancer [24]. In this study, we examined the correlation between C18orf54 gene expression and immune cells related to liver cancer, including $CD8^+$ T cells, $CD4^+$ T cells, macrophages, B cells, and neutrophils. *P*-value of less than 0.05 was considered statistically significant.

TISIDB

An integrated repository portal for tumor-immune system interactions (TISIDB) is a web portal for interactions between tumors and the immune system, integrating a variety of heterogeneous data types (http://cis.hku.hk/TISIDB/index.php). Interactions between tumors and the immune system play crucial roles in the

occurrence, progression, and treatment of cancer. Cytolytic immune cells (T/NK cells) are initially intended to recognize and kill cancer cells, while tumor tissues can shape the surrounding microenvironment to promote immune escape. Specifically, tumors can disrupt T/NK cell infiltration, T/NK cell function, and antigen presentation through soluble and cell surface mediators (like PD-L1) and immune suppressive cells (such as regulatory T cells (Tregs) and myeloid-derived suppressive cells (MDSCs)). Therefore, elucidating the interactions between tumor and immune cells will help predict immune treatment responses and develop new immune therapy targets. We used it to explore the interaction of C18orf54 with immune stimulators and inhibitors. To study the abundance of immune cell infiltration in HCC patients and the correlation of the C18orf54 gene with the abundance of immune cell infiltration, the Wilcoxon rank-sum test was used to calculate *p*-values and Spearman's rank correlation test was performed.

Clinical prognosis analysis

Data was sourced from The Cancer Genome Atlas (TCGA) (https://portal.gdc.cancer.gov/), specifically the Liver hepatocellular carcinoma (LIHC) project's level 3 HTSeq-FPKM formatted RNAseq data. RStudio software (v3.6.3) was used for statistical analysis and visualization of the data, with the ggplot2 package (3.3.3) used to draw the impact of C18orf54 on clinical prognosis indicators and survival time of hepatocellular carcinoma patients. A t-test was used for statistical analysis, with a *P*-value of less than 0.05 considered statistically significant.

CTD database

The Comparative Toxicogenomics Database (CTD) is a robust, publicly available database designed to advance understanding of how environmental exposures affect human health. It provides information on chemical-gene/protein interactions, chemical-disease, and gene-disease relationships. This data is combined with functional and pathway data to aid in the development of hypotheses about the potential mechanisms by which environmental factors influence disease (https://ctdbase.org/about/). We used it for the co-analysis of C18orf54 and drugs, and downloaded the BP, CC, MF, KEGG, etc., data of drugs interacting with C18orf54 and hepatocellular carcinoma for visualization.

DSigDB

The Drug Signatures Database (DSigDB) organizes drug and small molecule related gene sets into four collections based on quantitative gene expression data of drug perturbations. We also retrieved drugs interacting with C18orf54 from it. To obtain potential hepatocellular carcinoma (HCC) targeted therapeutic drugs, hub genes were imported into DGIdb (http://www.DGIdb.org), potential HCC related therapeutic drugs were obtained and their results were visualized.

Statistical analysis

All data statistical analyses were performed using R 3.6.3 and the corresponding R packages. Mainly included are the t-tests, Wilcoxon rank sum tests for comparing group differences, Spearman's rank correlation test for correlation analysis, Image J for quantitative analysis of morphology and protein band results, and patient related statistical data were analyzed with SPSS22.0 and GraphPad Prism 8.0 software. Depending on variable distribution, the t-test was used for two groups of counting data, with a *P*-value < 0.05 considered statistically significant.

Result

Combined analysis on multiple databases for new biological markers of HCC

The research design flow chart is in **Figure 1**. To find new biological markers of HCC, we used 4 HCC datasets from the GEO database (GSE84402, GSE101685, GSE61132, GSE1-12790) for a differential analysis, whose results were counted (**Table 1**) and visualized in a volcano plot (**Figure 2A**), meanwhile the upregulated differential genes in the 4 databases were intersected and plotted in a Venn diagram. We found that there were 192 co-regulated genes in the Wayne diagram (**Figure 2B**), and then used the co-regulated genes to correlate the enrichment of genes, finding that there were 123 co-expressed genes in biological functions (BPs), 55 in cellular components (CCs), 55 in molecular functions (MFs) and 60 in Kyoto Encyclopedia of Genes and Genomes

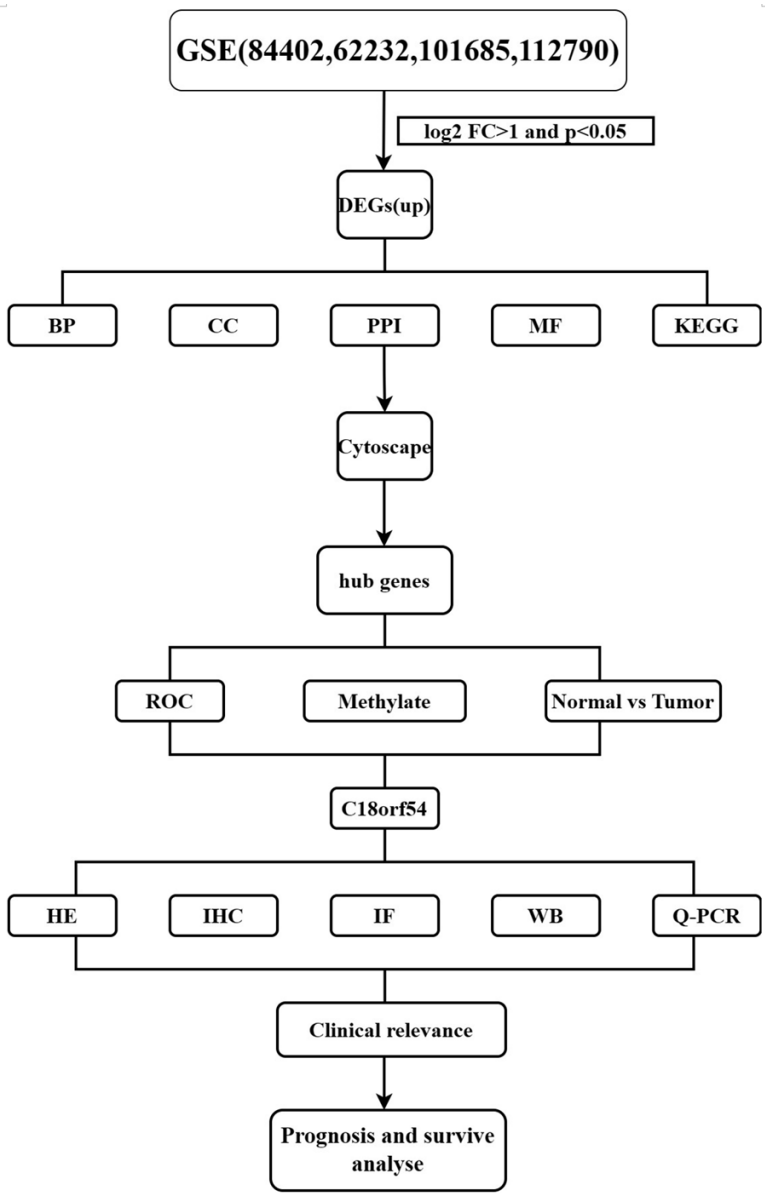

Figure 1. Research design flow chart. DEGs, Differential Expressed Genes; BP, Biologic processes; CC, Cell components; MF, Molecular functions; KEGG, Kyoto Encyclopedia of Genes and Genomes; PPI, Protein-protein interaction network; ROC, Receiver Operating Characteristic; C18orf54, Chromosome 18 Open Reading Frame 54; HE, Hematoxylin and Eosin staining; IHC, Immunohistochemical; IF, Immunofluorescence; WB, Western blot; Q-PCR, Real-time Quantitative PCR Detecting System.

(KEGG). The top 3 results of enrichment in BFs were cell division, cell cycle and mitotic cell cycle involved in DNA replication. The top 3 enrichment results of CCs were nucleus, cytosol and nucleoplasm. The top 3 enrichments in MFs were protein binding, ATP binding and identical protein binding (**Figure 3A**). The top 3 enrichments in KEGG were Cell cycle, DNA replication and Oocyte meiosis. We made a careful genetic differentiation of KEGG pathway enrichment by interlinking genes with enriched pathways, meanwhile PCNA/BUB1B/TTK/CDC6/CCNA2/CDC20/CCNB2/CCNB1/CCNE2/PTTG1/MCM3/CDK1/MCM4/MCM5/MCM6/MCM2/CDC20/CCNB2/CCNB1/PTTG1/CCNE2/CDK1/MAD2L1/AURKA MAD2L1/AURKA genes were enriched in the Cell cycle (**Figure 3B**, **3C**). Taken together, co-upregulated genes might be closely associated with tumorigenesis by regulating aspects of cell functions.

C18orf54 is a potential new biological target in HCC with methylation mutation sites

We submitted 192 differential genes to STRING online database, mapped a PPI network consisting of 190 nodes and 3657 edges (**Figure 4A**), visualized the results through Cytoscape software, and then used the MCODE app to screen 5 hub genes (**Figure 4B**), which were used for the next tissue-specific analysis. We continued to analyze the mRNA expression of hub gene in HCC and normal tissues, and BARD1 ($P < 0.001$), MSH2 ($P < 0.001$), H2AFX ($P < 0.001$), H2AFZ ($P < 0.001$) and C18orf54 ($P < 0.001$) were significantly up-regulated in HCC (**Figure 5A-E**). Given that aberrant DNA hypermethylation in gene promoter regions is the most well-defined epigenetic change in tumors that is associated with inappropriate gene silencing [25], we also performed a correlation analysis of methylation, where 5 methylation mutation sites were present in C18orf54 (**Figure 6A**, **6B**), 5 methylation mutation sites in BARD1 (Supplementary Figure 1B, 1C), 2 methylation

Table 1. Details of the GEO HCC data

	Total number of ID	*P* value < 0.05 |$\log_2$ FC| >1	High expression gene	Low expression gene	Platform
GSE84402	21652	1200	633	567	GPL570
GSE101685	21655	1687	826	861	GPL570
GSE62232	21655	1205	601	604	GPL570
GSE112790	21655	1440	815	625	GPL570

Abbreviations: HCC, Hepatocellular carcinoma; GEO, Gene Expression Omnibus database.

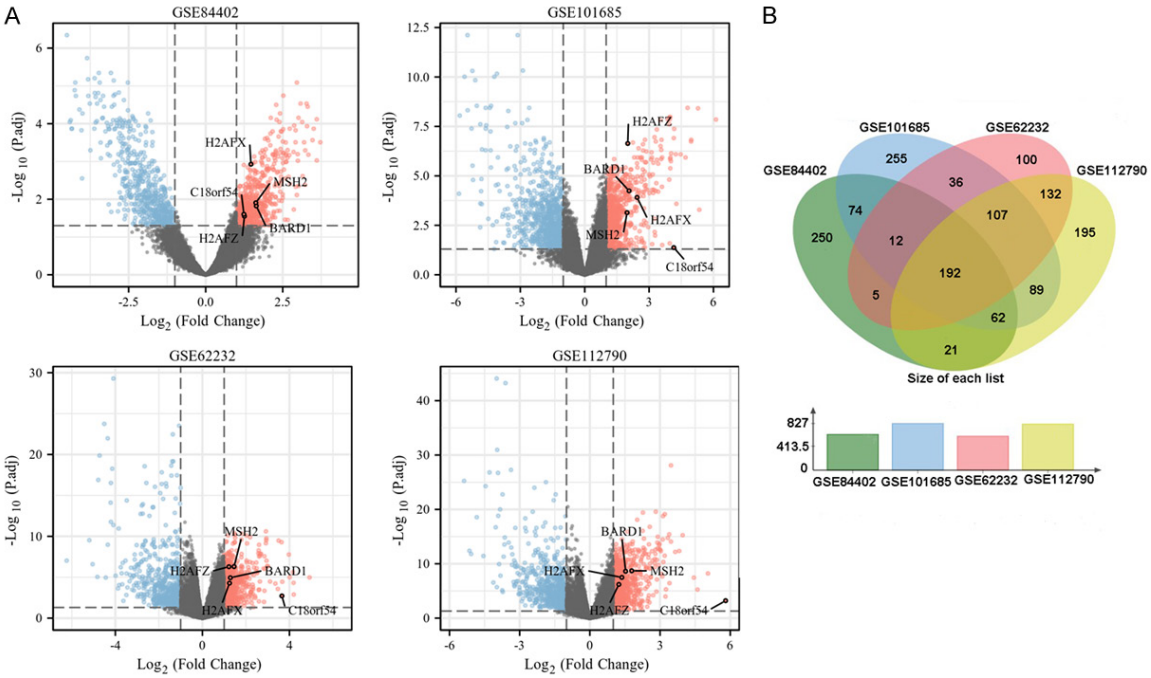

Figure 2. Combined analysis of multiple databases for new biological markers in HCC. A. GSE84402, GSE101685, GSE61132, GSE112790 volcano plots. B. Vinci cross plots between all genes of HCC obtained from 4 databases. MSH2, Mismatch Repair Protein; H2AFX, Recombinant H2A Histone Family, Member X; H2AFZ, Recombinant H2A Histone Family, Member Z; C18orf54, Chromosome 18 Open Reading Frame 54; HCC, Hepatocellular carcinoma.

mutation sites in MSH2 (Supplementary Figure 2A-C), 1 methylation mutation site in H2AFX (Supplementary Figure 2D, 2E), and 1 methylation mutation site in H2AFZ (Supplementary Figure 2F, 2G) (**Table 2**). Therefore, we speculated that C18orf54 affected the developmental progression of HCC, which might be related to the methylation mutation profile. In the existing studies, the relationship between the C18orf54 gene and HCC has not been explored and the associated molecular mechanisms are unclear. We initially screened C18orf54 as a potential biological target in HCC through a bioinformatics analysis, together with its possible relevance to the diagnosis, treatment and prognosis of HCC. The specific data on the methylation of the above hub genes is presented in **Table 2**.

C18orf54 shows a differentially-high expression in HCC

We searched the HPA database for C18orf54 expression in normal tissues and found it most highly expressed in testicular tissues (**Figure 7A**), then continued validating it in single cells of testicular tissues through the Single Cell Expression Atlas database (**Figure 7B**), and used the C18orf54 gene to overlay (**Figure 7C**). We then proceeded to validate in single cells of normal liver tissues (**Figure 7D**), and similarly, overlaying single cell tissues with the C18orf54 gene revealed that C18orf54 was barely expressed in normal livers (**Figure 7E**). Based on the HCC dataset, we validated the C18orf54 expression in HCC and found a large difference (P < 0.001) (**Figure 7F**). All these results sug-

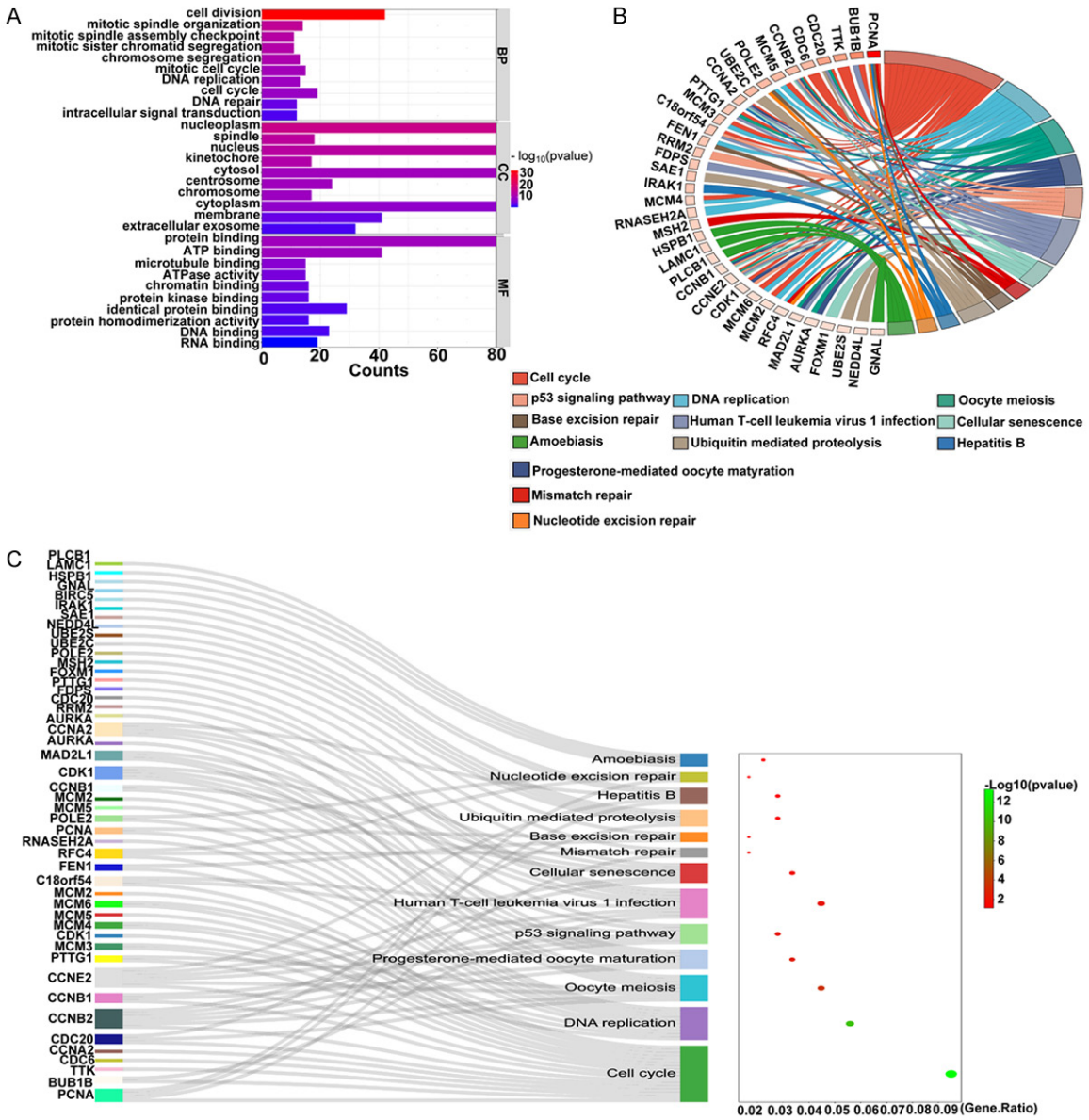

Figure 3. Multi-database joint analysis of differential gene pathway enrichment. A. BP, CC, MF. B. KEGG chord diagram. C. Proportion of pathways accounted for by the KEGG pathway. BARD1, BRCA1 associated RING domain 1; MSH2, Mismatch Repair Protein; H2AFX, Recombinant H2A Histone Family, Member X; H2AFZ, Recombinant H2A Histone Family, Member Z; C18orf54, Chromosome 18 Open Reading Frame 54; BP, Biologic processes; CC, Cell components; MF, Molecular functions; KEGG, Kyoto Encyclopedia of Genes and Genomes.

gest that C18orf54 expression is highly abnormal in liver tissues of patients with HCC, which is of concern.

Experimentally verified that C18orf54 showed a high expression in the liver tissues of patients with HCC

To observe the lesions in the sections of patients with HCC, after H&E staining, the hepatocellular carcinoma lesions were microscopically seen to have typical surfaces filled with diffuse nodules of varying sizes and collapsed areas of fibrous septa with the formation of larger multilocular regenerative nodules. Pseudo lobular complexes with a radial arrangement of hepatocytes were seen (**Figure 8A**). We wanted to further investigate the distribution and localization of the C18orf54 gene, and through immunohistochemical staining, C18orf54 was seen to have a significant positive expression in hepatocellular carcinoma

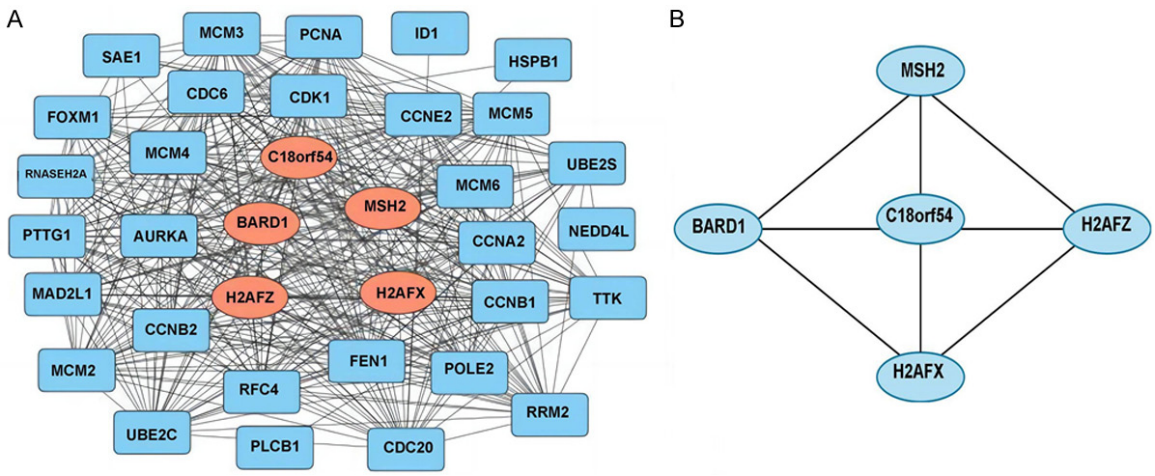

Figure 4. C18orf54 was found as a new biomarker of HCC. A. PPI interoperability network. B. The hub gene PPI network. BARD1, BRCA1 associated RING domain 1; MSH2, Mismatch Repair Protein; H2AFX, Recombinant H2A Histone Family, Member X; H2AFZ, Recombinant H2A Histone Family, Member Z; C18orf54, Chromosome 18 Open Reading Frame 54; HCC, Hepatocellular carcinoma; PPI, Protein-Protein Interaction Networks.

lesion tissues, with a strong positive expression of tan color around the lesions (**Figure 8B**), while no significant positive expression was seen in the control group ($P < 0.001$) (**Figure 8C**). After IF staining, C18orf54 had a significant positive expression in HCC liver tissues (**Figure 8D**), and we found it showing a diffuse distribution in hepatocellular carcinoma. We performed a protein and RNA extraction on specimens from patients with HCC, and WB results showed that the protein content of C18orf54 was significantly higher in tissues of patients with HCC than in control samples ($P < 0.001$) (**Figure 8F**), as is shown in **Figure 8E**, and finally, PCR results showed that C18orf54 mRNA expression was significantly higher ($P < 0.001$) in HCC samples compared with the corresponding non-tumor samples (**Figure 8G**). Taken together, the experiments showed that C18orf54 was significantly different between liver tissues of patients with HCC and normal tissues, suggesting that C18orf54 may serve as a new biomarker of HCC.

C18orf54 is involved in HCC immune cell infiltration through the depletion of CD4⁺ T cells and macrophages

To understand how C18orf54 promotes the progression of HCC and whether it is associated with tumor immunity, we explored C18orf54 and immune cell infiltration in HCC using Timer 2.0. We found that in HCC, C18orf54 expression was associated with the infiltration of $CD8^+$ T cells ($P < 0.001$), $CD4^+$ T cells ($P < 0.001$), T cell regulatory ($P < 0.001$), B cells ($P < 0.001$), macrophages ($P < 0.001$), Neutrophils ($P < 0.001$), NK cell activated ($P < 0.001$) and Cancer associated fibroblast ($P < 0.001$) whose levels were negatively correlated (**Figure 9A-H**). The above results indicated that C18orf54 expression correlated with the depletion of immune cells in HCC, and after visualizing the significant degree, we found that C18orf54 expression was most significantly negatively correlated with the level of infiltration of $CD4^+$ T cells and macrophages (**Figure 10A**). Immediately after, we found that patients with HCC, with a high expression of C18orf54, a low expression of $CD4^+$ T cells and macrophages, had a shorter survival and worse prognosis in terms of duration and tumor stage (**Figure 10B-E**). In summary, we found that a high expression of C18orf54 might affect the survival and prognosis of patients with HCC by depleting immune cells, especially $CD4^+$ T cells and macrophages. Specific data on C18orf54 immune infiltrating cells is available in Supplementary Figure 3 and **Table 3**.

C18orf54 correlates with immune checkpoints (immunosuppressants)

Since C18orf54 may be involved in tumor immunity, we further explored the relationship between C18orf54 and immune checkpoints, especially immunosuppressants, which we investigated using the TISIB database and

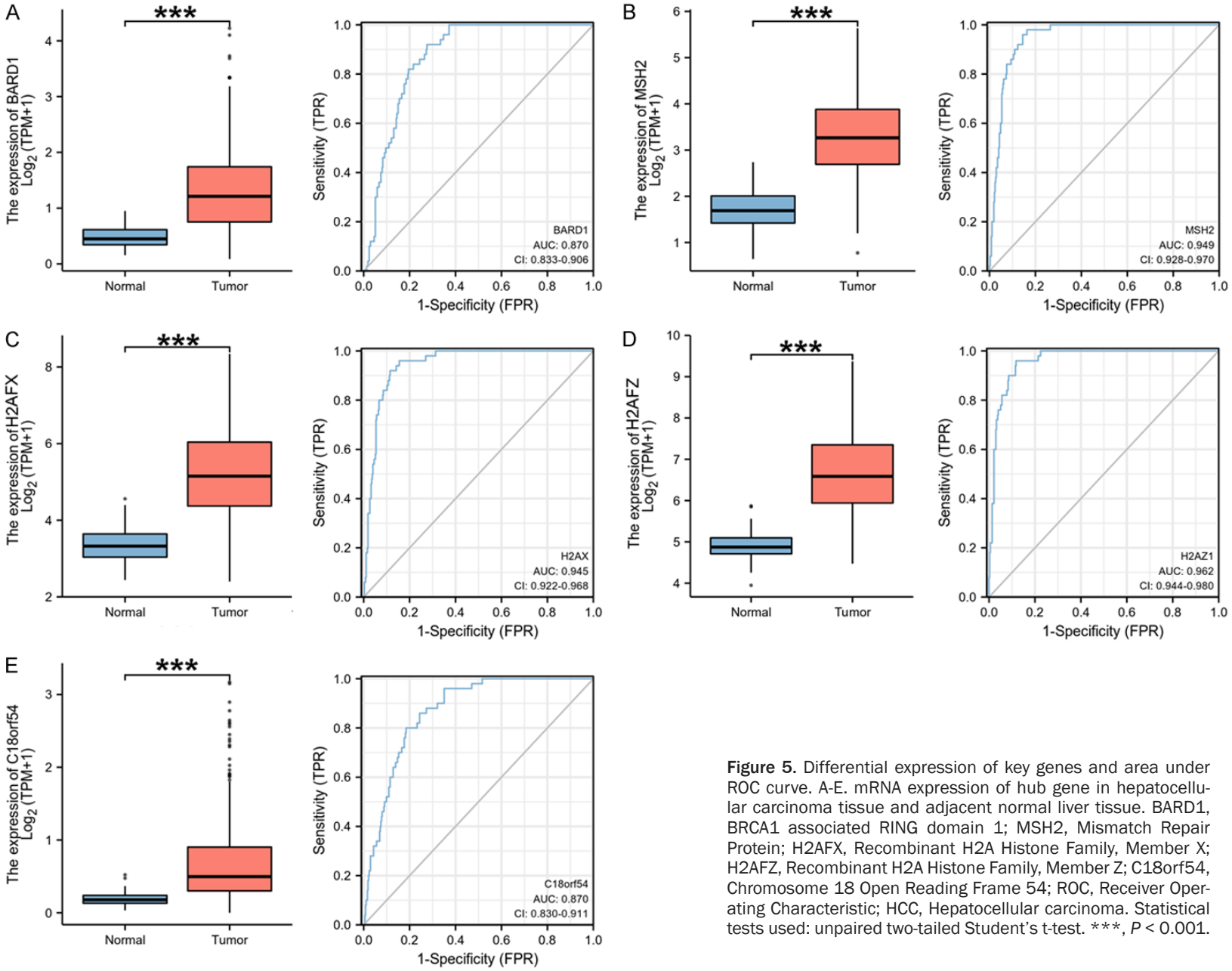

Figure 5. Differential expression of key genes and area under ROC curve. A-E. mRNA expression of hub gene in hepatocellular carcinoma tissue and adjacent normal liver tissue. BARD1, BRCA1 associated RING domain 1; MSH2, Mismatch Repair Protein; H2AFX, Recombinant H2A Histone Family, Member X; H2AFZ, Recombinant H2A Histone Family, Member Z; C18orf54, Chromosome 18 Open Reading Frame 54; ROC, Receiver Operating Characteristic; HCC, Hepatocellular carcinoma. Statistical tests used: unpaired two-tailed Student's t-test. ***, $P < 0.001$.

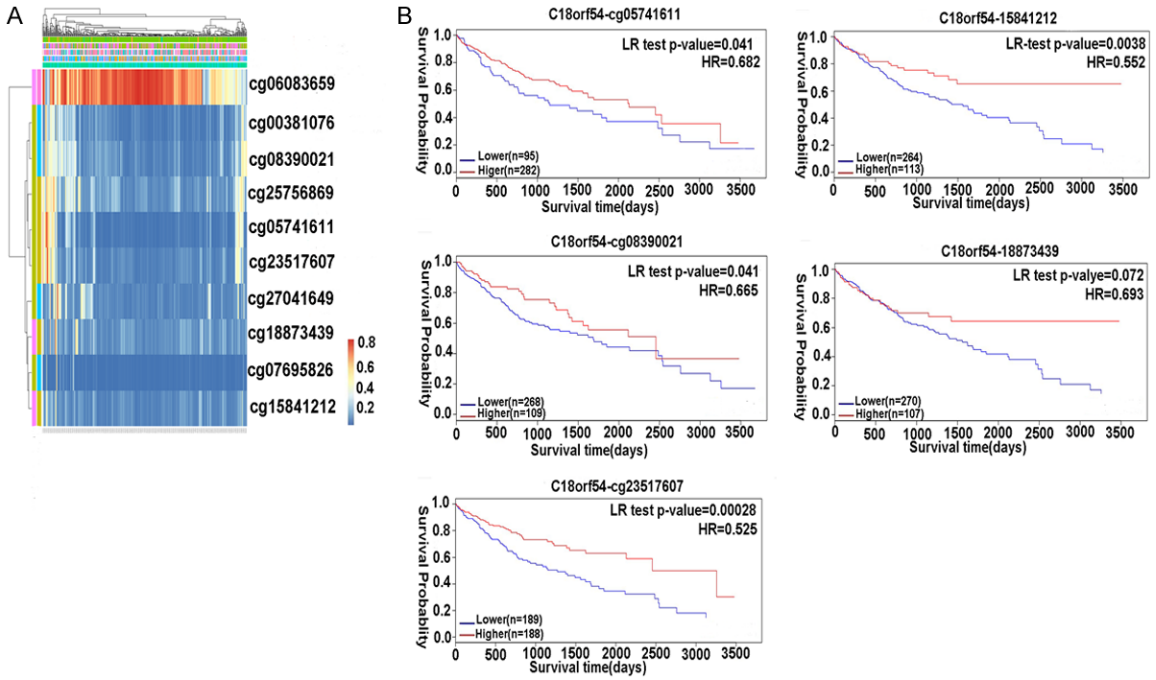

Figure 6. Study on methylation site of C18orf54 in HCC. A. CpG clustering analysis of C18orf54 heat map with methylation levels associated with patient characteristics and genetic subregions. B. Prognosis of the CpG locus of C18orf54 in HCC patients. LR, likelihood ratio; HR, Hazard Ratio; C18orf54, Chromosome 18 Open Reading Frame 54; HCC, Hepatocellular carcinoma.

Table 2. Gene methylation status of hub

p	BARD1	MSH2	H2AFX	H2AFZ	C18orf54
Cg02172142	0.011				
Cg04004882	0.019				
Cg08563601	0.0053				
Cg19237985	0.0011				
Cg23075101	0.012				
Cg11311499		0.028			
Cg14282180		0.00015			
Cg04208787			< 0.001		
Cg17709884				0.005	
Cg05741611					0.041
Cg08390021					0.041
Cg15841212					0.0038
Cg23517607					0.00028
Cg18873439					0.072

Abbreviations: BARD1, BRCA1 associated RING domain 1; MSH2, Mismatch Repair Protein; H2AFX, Recombinant H2A Histone Family, Member X; H2AFZ, Recombinant H2A Histone Family, Member Z; C18orf54, Chromosome 18 Open Reading Frame 54.

found that C18orf54 was associated with 16 immunosuppressants (**Table 4**) (**Figure 11A-Q**), of which the top 3 correlations were Hepatitis A virus cellular receptor 2 (HAVCR2), T cell immunoreceptor with Ig and ITIM domains (TIGIT) and Cytotoxic T lymphocyte associate protein-4 (CTLA4), and the associated immunosuppressants could be used as potential immunotherapeutic targets of HCC. In addition, we explored the relationship of immunostimulants and MHC

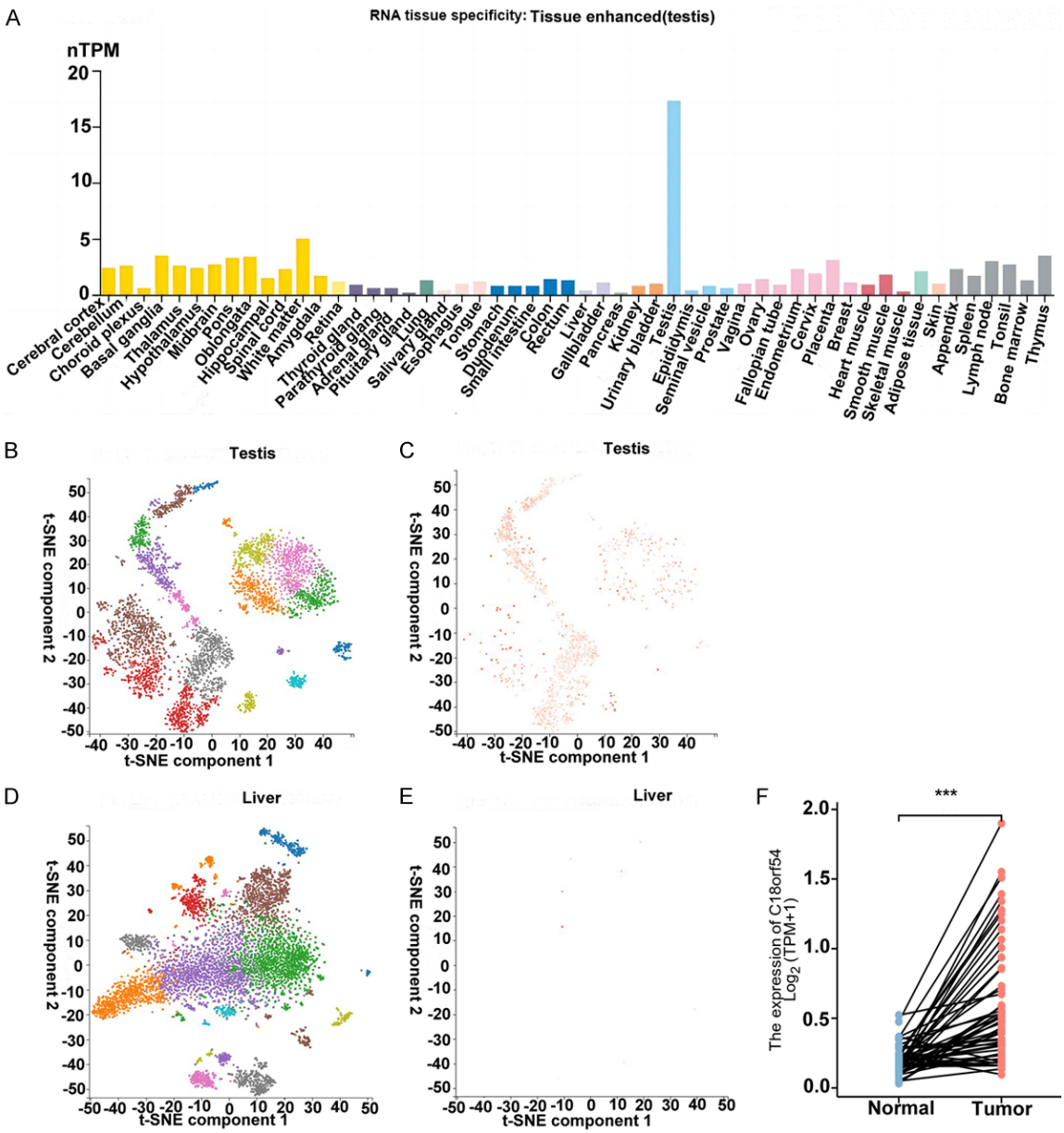

Figure 7. C18orf54 shows differential high expression in HCC. A. Expression of C18orf54 in normal tissues. B. Cellular expression in testicular tissues. C. Expression of C18orf54 in testicular tissues. D. Cellular expression in hepatocellular carcinoma tissues. E. Expression of C18orf54 in liver tissues. F. Based on TCGA dataset, we verified the expression of C18orf54 in HCC. LR, likelihood ratio; HR, Hazard Ratio; C18orf54, Chromosome 18 Open Reading Frame 54; HCC, Hepatocellular carcinoma. Statistical tests used: unpaired two-tailed Student's t-test. ***, $P < 0.001$.

molecular targets with C18orf54 in Supplementary Figures 4, 5 and Specific statistics in **Tables 5**, **6**.

A higher expression of C18orf54 is associated with a worse prognosis and survival

HCC progression is usually accompanied by an abnormal gene expression and a poor prognosis, and key genes in HCC progression are usually associated with cancer stages and patient prognosis. We also investigated C18orf54 and the survival time, stage as well as grade of patients with HCC, finding that patients with HCC and a high C18orf54 expression had a shorter survival time (**Figure 12A**, **12B**), C18orf54 expression was significantly higher in Stage III and IV of tumor stages (**Figure 12C**,

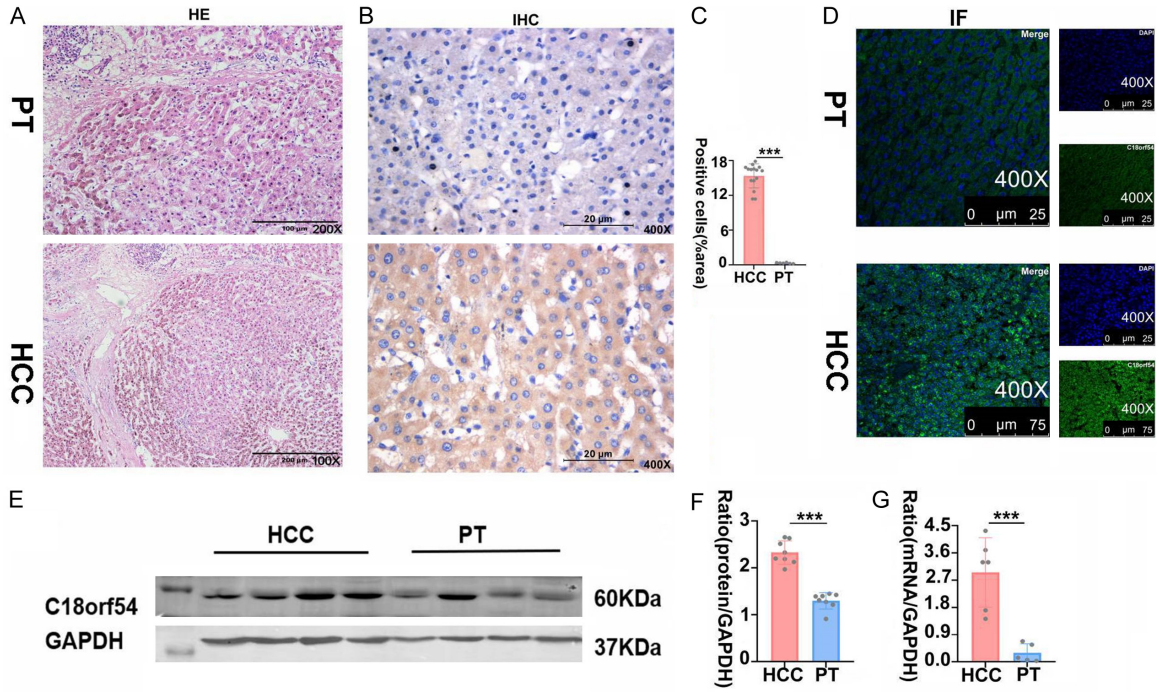

Figure 8. Experimentally verified that C18orf54 showed high expression in the liver tissue of HCC patients. A. PT (200×) and HCC (100×) in H&E staining. B. PT and HCC in IHC staining (400×). C. Immunohistochemistry statistics in IHC. D. PT and HCC in IF (400×). E. PT and HCC in WB. F. Statistics in WB. G. PT and HCC in RT-PCR Statistical results. PT, Remote control tissue of tumor patients; HCC, hepatocellular carcinoma; HE, Hematoxylin and Eosin staining; IHC, Immunohistochemical; IF, Immunofluorescence; C18orf54, Chromosome 18 Open Reading Frame 54. Statistical tests used: unpaired two-tailed Student's t-test. ***, $P < 0.001$.

12D). The expression of C18orf54 was significantly increased in grade 3 and I4 of hepatocellular carcinoma (**Figure 12E**, **12F**). Taken together, the study showed that a high stable C18orf54 was associated with the progression of HCC, signifying a worse prognosis and a shorter survival time. An analysis of our C18orf54 with, overall survival (OS) and disease specific survival (DSS) in patients with HCC also yielded consistent results, reinforcing our study (**Figure 13A**, **13B**). Calibration plots showed that the column line graph model was used to predict the probability of survival after 1, 2 and 3 years, showing a high agreement with the actually-observed survival probability and a high fit with the predicted death line, reinforcing the prognostic value of C18orf54 in HCC (**Figure 13C-F**). We also analyzed clinical indicators of C18orf54, including a higher incidence of adjacent liver tissue inflammation, higher child-Pugh grade scores, and higher rates of residual tumor recurrence in patients with hepatocellular carcinoma (Supplementary Figure 6A-P) (**Table 7**). Similarly, the prognosis was worse in the subset of patients (Supplementary Figure 7A-M) (**Table 8**).

Potential drug targets of C18orf54 in HCC

We searched for drugs interacting with C18orf54 from the CTD database and downloaded the data for drug enrichment, finding that the top 3 results of biological function (BF) enrichment were a negative regulation of cell population proliferation, a positive regulation of transcription via RNA polymerase II and a positive regulation of transcription using a nucleic acid template, while the top 3 results of cellular component CC enrichment were extracellular regions, intracellular organelles and intracellular organelles without membrane restriction, which also matched our CC results of the enrichment of worker upregulated genes, providing more evidence that C18orf54 was a secretory molecule and that the top 3 molecular functions (MFs) enriched were protein binding, sequence-specific double-stranded DNA binding as well as adenosine nucleotide binding to exert drug action, followed by the enrichment visualization of drug action pathways, which resulted in prostaglandin-like ligand receptors, pentose phosphate pathways (hexose monophosphate shunt) and the generation

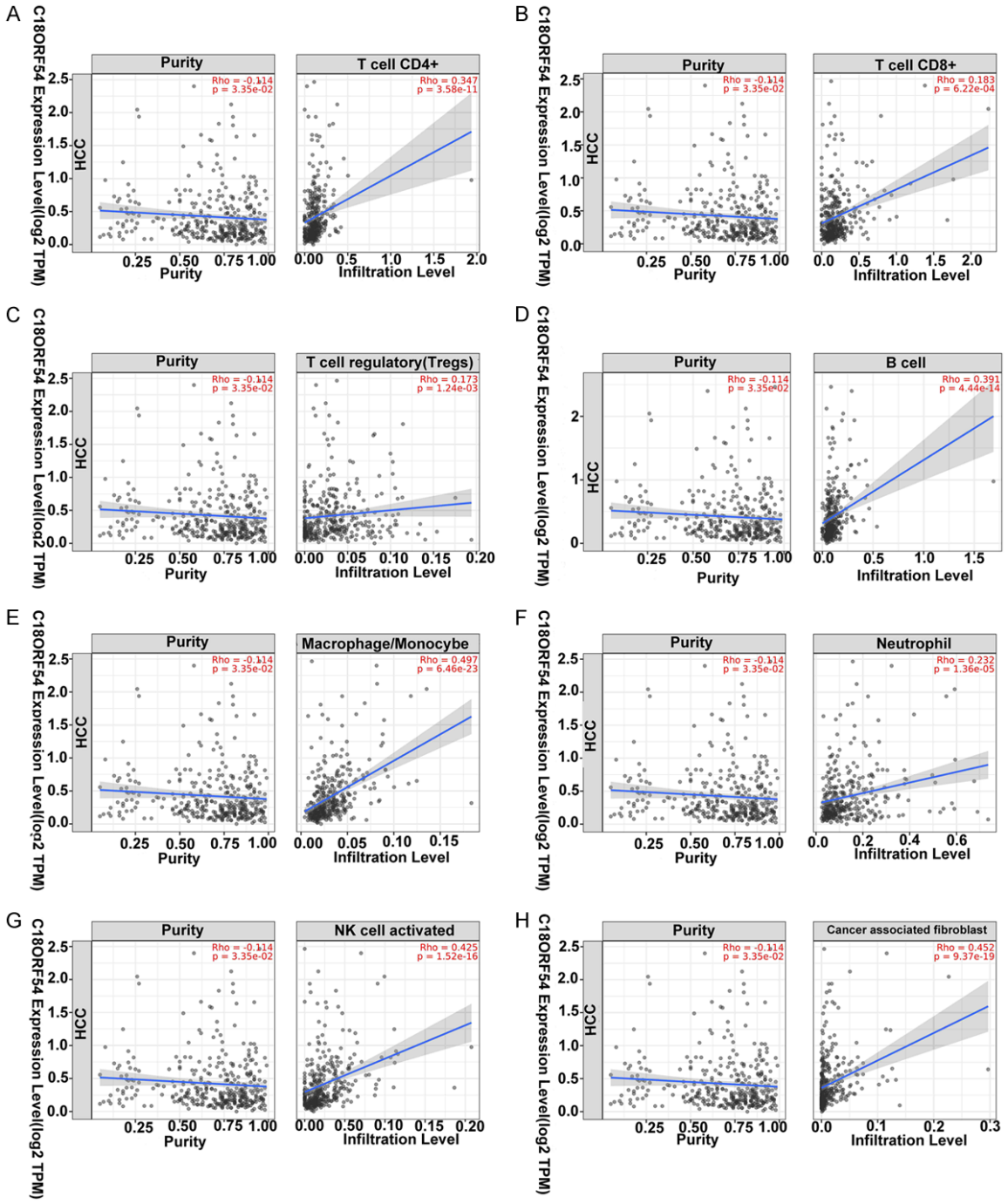

Figure 9. C18orf54 participates in the infiltration of HCC immune cells. A-H. Relationship between C18orf54 and eight types of immune infiltrates ($CD4^+$ T cells, $CD8^+$ T cells, T cell regulatory, B cells, Macrophages, Neutrophils, NK cell activated and Cancer associated fibroblast). HCC, Hepatocellular carcinoma; C18orf54, Chromosome 18 Open Reading Frame 54; rh0, regression coefficient.

of p75NTR regulation axon, etc. (**Figure 14A**, **14B**). We also analyzed the drug components most strongly associated with C18orf54, such as C5ORF34, PGBD1 and PNMA6A (**Figure 14C**). We also searched the DSigDB database for drugs that interacted with C18orf54 and intersected with drugs in the CTD database, finding that 4 drugs overlapped (**Figure 14D**), which were cyclosporine, calcitriol, quercetin and testosterone (**Figure 14E**), all of which can

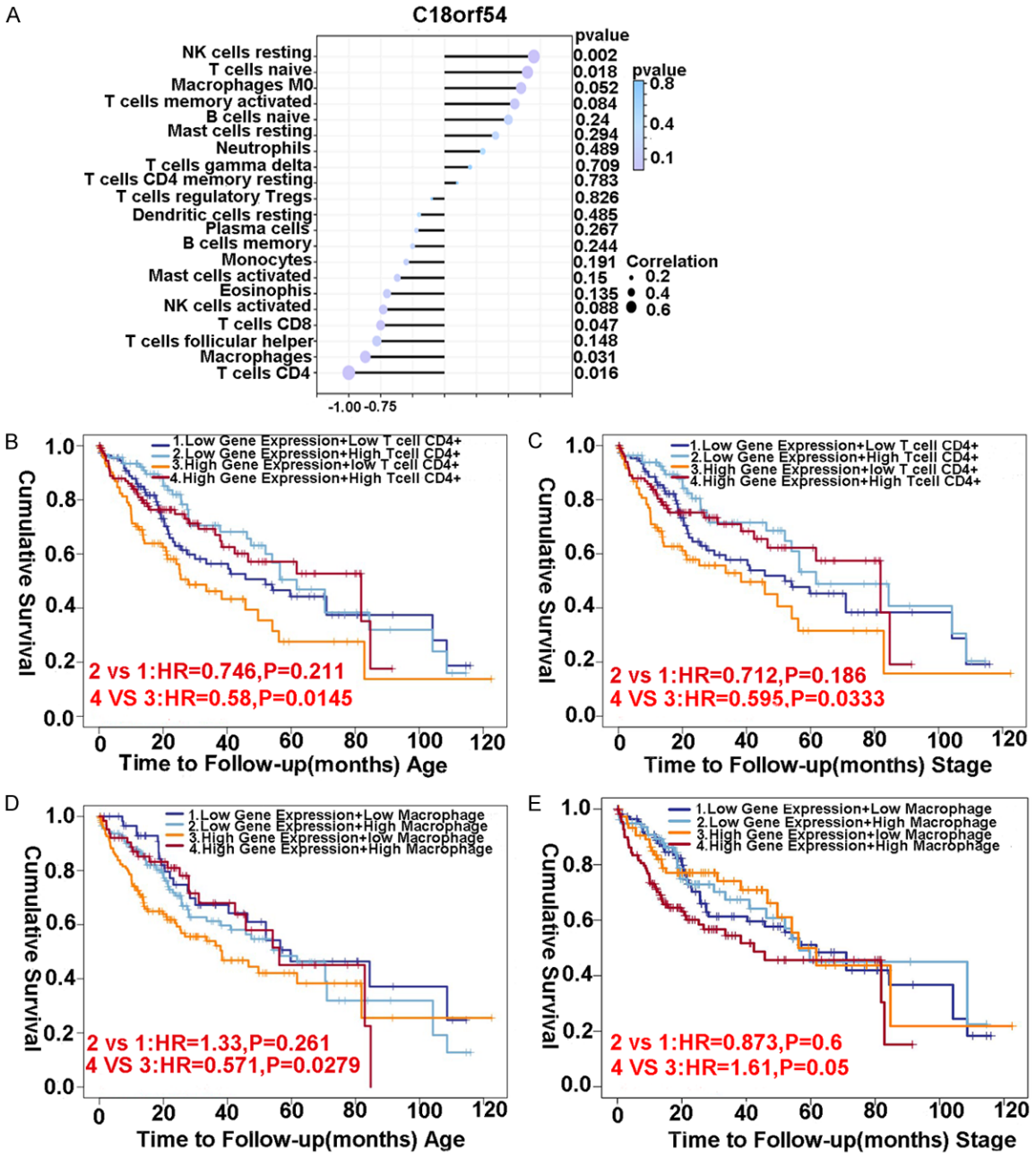

Figure 10. C18orf54 is involved in HCC immune cell infiltration through depletion of $CD4^+$ T cells and macrophages. A. Lollipop plot of C18orf54 and immune cell infiltration. B, C. Age and Stage prognostic analysis of C18orf54 associated with macrophage infiltration. D, E. Age and Stage prognostic analysis of C18orf54 associated with $CD4^+$ T cells. HCC, Hepatocellular carcinoma; C18orf54, Chromosome 18 Open Reading Frame 54; rh0, regression coefficient; HR, Hazard Ratio.

reduce the expression of C18orf54 mRNA, thus also providing us a new potential drug target for the treatment of liver cancers.

Discussion

Liver cancer is currently the second leading cause of cancer-related deaths worldwide [26], and HCC, which accounts for more than 90% of liver cancers, is one of the most common malignancies with a high probability of metastasis and recurrence [27], immunotherapy and systemic therapy remain the best treatment options for patients with HCC, given that most patients with HCC are diagnosed at intermediate to late stages and surgical resection is not

Table 3. Infiltration of C18orf54 immune cells

C18orf54	*P* value	rho
Act CD8	0.02	0.121
Act CD4	< 0.001	0.577
Tcm CD4	< 0.001	0.248
Tem CD4	< 0.001	0.295
Tfh	< 0.001	0.305
Tgd	< 0.001	0.141
Th1	0.0108	0.132
Th17	< 0.001	0.205
Th2	< 0.001	0.463
Treg	< 0.001	0.253
Act B	< 0.001	0.209
Lmm B	< 0.001	0.3
NKT	< 0.001	0.328
Act NKT	0.0131	0.128
Macrophage	< 0.001	0.208
Neutrophil	0.0027	0.155

Abbreviations: rh0, regression coefficient; C18orf54, Chromosome 18 Open Reading Frame 54.

Table 4. C18orf54 immunosuppressant site

C18orf54	*P* value	rho
ADORA2A	0.0186	0.122
BTLA	< 0.001	0.207
CD96	< 0.001	0.294
CSF1R	< 0.001	0.246
CTLA4	< 0.001	0.346
HAVCR2	< 0.001	0.393
IDO1	0.0033	0.152
KDR	< 0.001	-0.212
LAG3	0.00172	0.162
LGALS9	< 0.001	0.326
PDCD1	< 0.001	0.316
PDCD1L	< 0.001	0.154
TGFB1	< 0.001	0.309
TGFBR1	0.0421	0.105
TIGIT	< 0.001	0.349
VTCN1	< 0.001	0.216

Abbreviations: rh0, regression coefficient; C18orf54, Chromosome 18 Open Reading Frame 54.

an optimal option. However, these treatment options are associated with various side-effects, a heavy financial burden and poor prognostic outcomes [28]. Therefore, its urgent to identify sensitive and reliable prognostic biomarkers to identify patients with poor prognosis and those who can benefit from early adjuvants rather than salvage therapies. In recent years, an increasing number of studies have been focused on the molecular characterization of early diagnosis and prognosis. In our study, multiple databases were combined to identify key genes associated with immune cell infiltration in HCC, which are considered to be independent prognostic biomarkers for patients with HCC.

We combined multiple GEO HCC databases to screen differentially-upregulated genes and performed an enrichment analysis to show that common genes were enriched in regulating cellular functions, suggesting that they were closely associated with tumorigenesis. Then, we constructed a PPI network to identify hub genes using Cytoscape, which were BRCA1 associated RING domain 1 (BARD1), Mismatch Repair Protein (MSH2), Recombinant H2A Histone Family, Member X (H2AFX), Recombinant H2A Histone Family, Member z (H2AFZ) and Chromosome 18 Open Reading Frame 54 (C18orf54).

Relevant studies have shown that mutations and epigenetic modifications of the BARD1 gene lead to loss of tumor suppressor function, which in turn favors the development of HCC, and relevant experiments have also confirmed that upregulated BARD1 is significantly associated with lower survival and advanced stages in HCC patients, and it may promote cellular by targeting Akt signaling proliferation, invasion and migration, thus promoting hepatocarcinogenesis [17]. MSH2, an important DNA mismatch repair gene, maintains genomic stability through DNA replication errors, and related findings provide MSH2 as a new prognostic biomarker for HCC patients [18]. Overexpressed H2AFX may be involved in the regulation of tumor immunity by modulating immune cells in HCC [19]. H2AFZ overexpression is associated with multiple clinicopathological features, including pathological T-stage and tumor grade of HCC, it occurs in most HCC cases and warrants further clinical validation as a potential diagnostic and prognostic marker [20]. The expression of C18orf54 gene in HCC has not been explored yet. We combined three reasons to decide the C18orf54 gene as a potential biological target. First, we found that there are five methylation mutation sites of C18orf54 in hub gene, and RNA methylation and its associated downstream signaling pathways, including cell differentiation, sex determination and stress

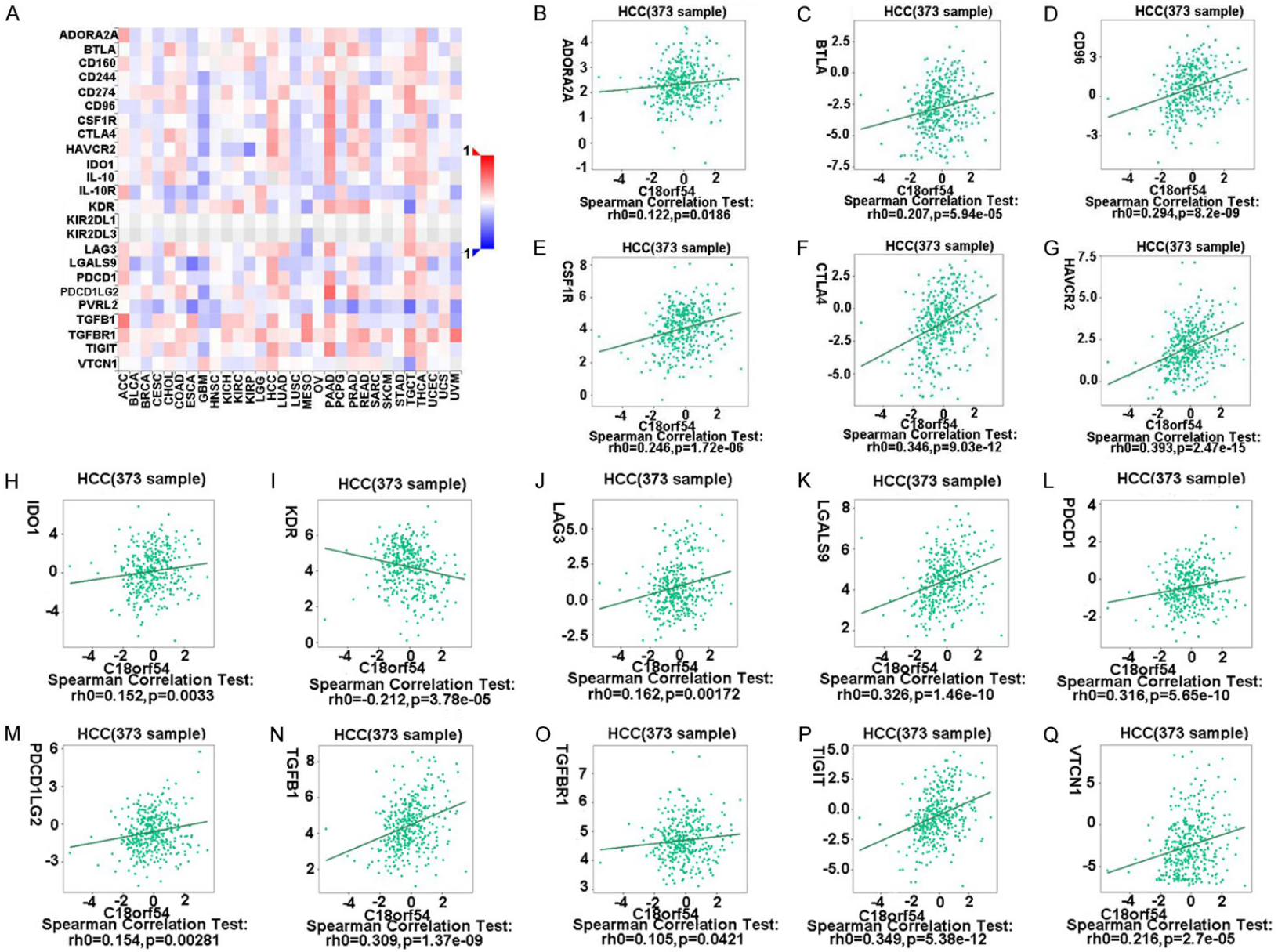

Figure 11. Correlation of C18orf54 with immune checkpoints (immunosuppressants). A. Heat map of the correlation between C18orf54 and immunosuppressive sites in pan-cancer. B-Q. Relationship between C18orf54 in HCC and each immunosuppressive site. HCC, Hepatocellular carcinoma; C18orf54, Chromosome 18 Open Reading Frame 54; rh0, regression coefficient.

Table 5. C18orf54 immunostimulant site

C18orf54	*P* value	rho
C10orf54	0.0091	0.135
CD27	< 0.001	0.284
CD276	< 0.001	0.281
CD28	< 0.001	0.253
CD40L	< 0.001	0.209
CD40LG	< 0.001	0.209
CD48	< 0.001	0.242
CD80	< 0.001	0.372
CD86	< 0.001	0.364
CXCR4	< 0.001	0.347
ENTPD1	< 0.001	0.258
HHLA2	< 0.001	0.281
ICOS	< 0.001	0.332
KLRK1	0.0166	0.124
MICB	< 0.001	0.234
LTA	< 0.001	0.334

Abbreviations: rh0, regression coefficient; C18orf54, Chromosome 18 Open Reading Frame 54.

Table 6. Relationship between C18orf54 and MHC I/II target

C18orf54	*P* value	rho
B2M	0.0091	0.135
HLA-DOB	< 0.001	0.284
HLA-DPA1	< 0.001	0.281
HLA-DPB1	< 0.001	0.253
HLA-DRA	< 0.001	0.209
HLA-DQA1	< 0.001	0.209
HLA-DQA2	< 0.001	0.242
HLA-DQB1	< 0.001	0.372
TAPBP	< 0.001	0.364
HLA-DRA	< 0.001	0.347
HLA-DRB1	< 0.001	0.258
TAP1	< 0.001	0.281

Abbreviations: C18orf54, Chromosome 18 Open Reading Frame 54; rh0, regression coefficient; MHC I/II, Major Histocompatibility Complex I/II.

response. It is catalyzed by RNA methyltransferases, demethylated by demethylases (FTO and ALKBH5), and read by methylation binding proteins (YTHDF1 and IGF2BP1), a process closely associated with cancer cell proliferation, cellular stress, metastasis, and immune response. RNA methylation-associated proteins have emerged as promising targets for cancer therapy [29]. Secondly, the ROC curve analysis of C18orf54 showed its high sensitivity and specificity for the diagnosis of HCC (AUC=0.87), and finally much evidence has showed that the remaining 4 hub genes have been validated as biological indicators of HCC, while C18orf54 did not point out its correlation with HCC in the currently-available studies, therefore, we started further exploring the biological characteristics and potential targets of C18orf54 in HCC.

To further investigate the relationship between C18orf54 and HCC, single-cell sequencing revealed that C18orf54 was highly expressed in normal human testicular tissues, which, was hardly expressed in normal livers, but its abnormal expression was associated with HCC. We speculated that the differential expression of C18orf54 could help us diagnose and predict HCC more accurately. Next, we clarified that both protein and gene level of C18orf54 showed a high expression in the related basic studies. Then we explored the immune infiltration of C18orf54 in HCC. Poor prognosis of HCC is usually associated with high levels of $CD4^+$ T cells and macrophages [30], and we found that the expression of C18orf54 was most negatively correlated with the degree of infiltration of $CD4^+$ T cells and macrophages, and even, HCC patients with high expression of C18orf54 and low expression of $CD4^+$ T cells and macrophages had shorter survival in terms of duration and tumor stage had a shorter survival and worse prognosis.

Given the role $CD4^+$ T cells play in orchestrating the responses by each of these cell types, the potential impact that exhaustion might have amidst the tumor-infiltrating or even systemic $CD4^+$ T cells population is substantial. Likewise, the direct cytotoxic role that $CD4^+$ T cells can have in mediating antitumor immunity [31-33] makes them a particularly germane population in cancer. As an extension, restoration of exhausted $CD4^+$ T cell function by checkpoint blockade, if feasible, may contribute significant clinical benefit in tumors, either by improving direct $CD4^+$ T cell antitumor activity or increasing $CD4^+$ T cell helper functions [34]. This can also be confirmed with our findings, where we speculated that C18orf54 might cause increased tumor activity in patients with HCC through depletion of $CD4^+$ T cells, with worse survival and prognosis. Macrophage overexpression is strongly associated with poor

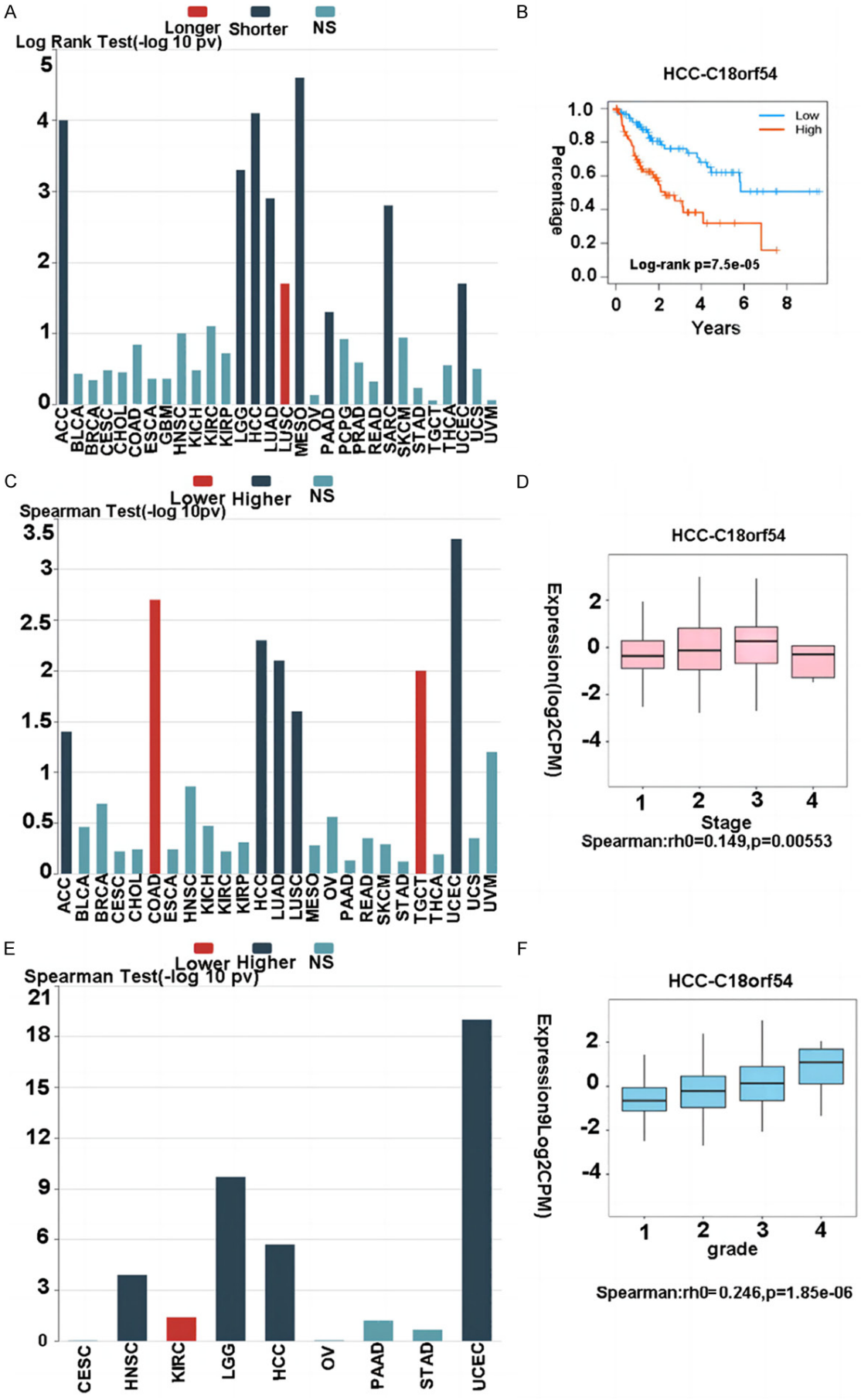
A
Longer
Shorter
NS
Log Rank Test(-log 10 pv)
ACC BLCA BRCA CESC CHOL COAD ESCA GBM HNSC KICH KIRC KIRP LGG HCC LUAD LUSC MESO OV PAAD PCPG PRAD READ SARC SKCM STAD TGCT THCA UCEC UCS UVM
B
HCC-C18orf54
Low
High
Percentage
Log-rank p=7.5e-05
Years
C
Lower
Higher
NS
Spearman Test(-log 10pv)
ACC BLCA BRCA CESC CHOL COAD ESCA HNSC KICH KIRC KIRP HCC LUAD LUSC MESO OV PAAD READ SKCM STAD TGCT THCA UCEC UCS UVM
D
HCC-C18orf54
Expression(log2CPM)
Stage
Spearman:rh0=0.149,p=0.00553
E
Lower
Higher
NS
Spearman Test(-log 10 pv)
CESC HNSC KIRC LGG HCC OV PAAD STAD UCEC
F
HCC-C18orf54
Expression9Log2CPM)
grade
Spearman:rh0=0.246,p=1.85e-06

Figure 12. High expression of C18orf54 is associated with worse prognosis and survival. A, B. Expression of C18orf54 in pan-cancer, and shorter survival time for high expression of C18orf54 in HCC. C, D. Expression of C18orf54 in pancytopenia and higher Stage III C18orf54 expression in HCC. E, F. Expression of C18orf54 in pancytopenia and higher grade 3/4 C18orf54 expression in HCC. HCC, hepatocellular carcinoma; C18orf54, Chromosome 18 Open Reading Frame 54; OS, overall survival; DSS, disease specific survival.

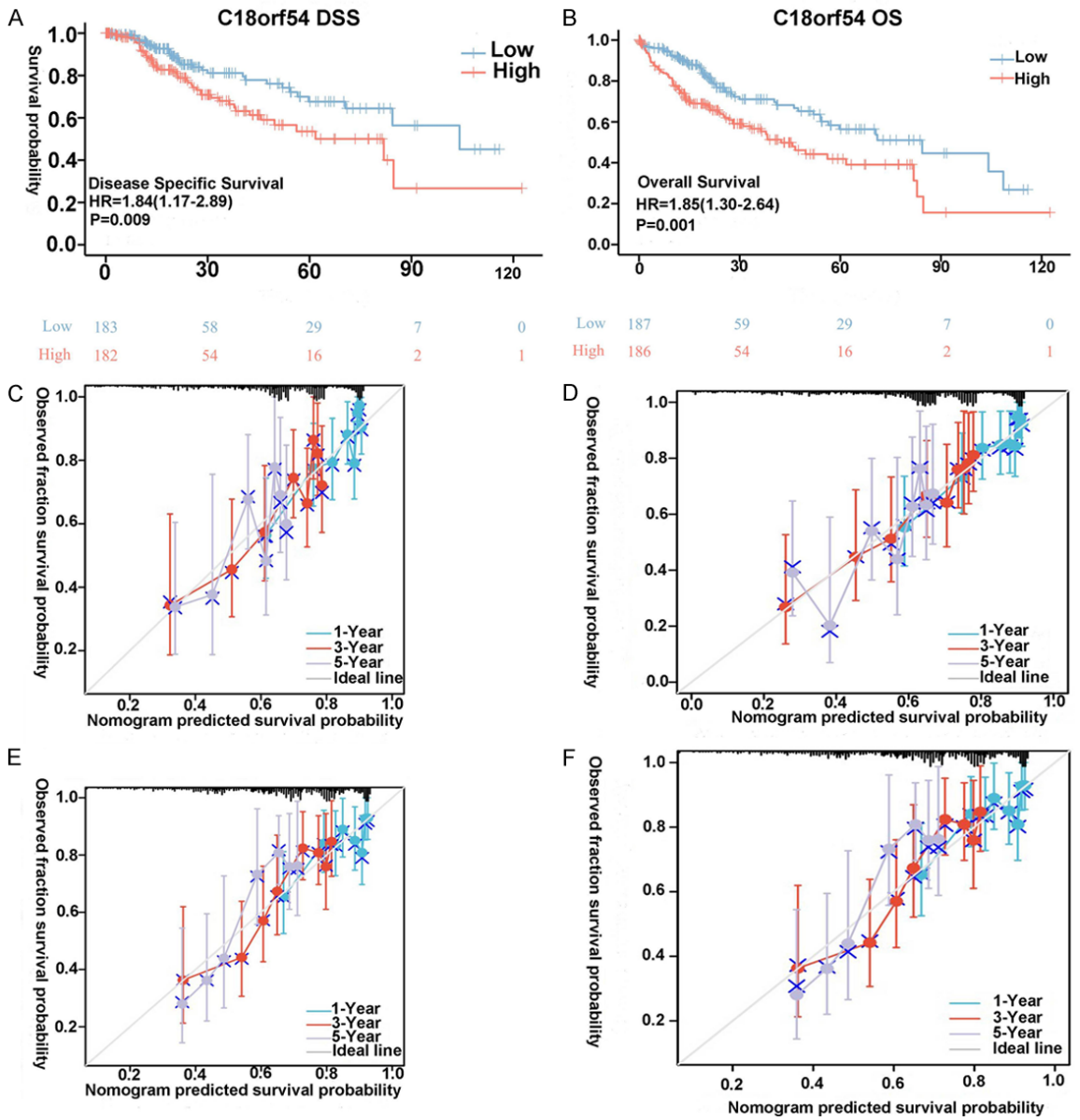

Figure 13. The survival probability of HCC patients with high expression of C18orf54 is lower. A, B. OS and DSS analysis of C18orf54. C-F. Columnar graphical models predicting the probability of survival at 1, 2 and 3 years C18orf54 with Tumor Status, T stage, Pathologic Stage. HCC, hepatocellular carcinoma; C18orf54, Chromosome 18 Open Reading Frame 54; OS, overall survival; DSS, disease specific survival.

prognostic survival, and macrophages can contribute to tumor cell escape into the circulatory system, suppress antitumor immune mechanisms and responses, and promote adaptive immune responses [35-37]. Recently, immunotherapeutic strategies, particularly immune checkpoint blockade therapy, have been considered as promising options for the treatment of various malignancies, including HCC [38, 39]. Therefore, exploring new immune biomark-

Table 7. Clinical data characteristics of C18orf54

Characteristics	Total (N)	Odds Ratio (OR)	*P* value
T stage (T1/T2/T3/T4 vs Normal)	371	1.970 (1.223-3.210)	< 0.001
Pathologic stage (Stage I/Stage II/Stage III/Stage IV vs Normal)	350	2.077 (1.277-3.419)	< 0.001
Tumor status (With tumor/Tumor free vs Normal)	355	1.275 (0.838-1.945)	< 0.001
Age (>60/≤60 vs Normal)	373	0.576 (0.381-0.867)	< 0.001
Age (>60 vs ≤60)	373	0.576 (0.381-0.867)	< 0.05
Residual tumor (R1/R0 vs Normal)	344	3.562 (1.231-12.855)	< 0.001
Residual tumor (R1 vs R0)	344	3.562 (1.231-12.855)	< 0.05
Histologic grade (G1/G2/G3/G4 vs Normal)	369	2.083 (1.357-3.219)	< 0.001
Histologic grade (G1 vs G3)	369	2.083 (1.357-3.219)	< 0.001
Histologic grade (G1 vs G4)	369	2.083 (1.357-3.219)	< 0.05
Adjacent hepatic tissue inflammation (Mild/Severe/None and Normal)	237	1.128 (0.676-1.884)	< 0.001
AFP (ng/ml) (>400/≤400 and Normal)	280	2.801 (1.576-5.110)	< 0.001
AFP (ng/ml) (>400 and ≤400)	280	2.801 (1.576-5.110)	< 0.01
Albumin (g/dl) (≥3.5/< 3.5 vs Normal)	300	1.276 (0.743-2.210)	< 0.001
Prothrombin time (>4/≤4 vs Normal)	297	0.654 (0.393-1.078)	< 0.001
Child-Pugh grade (A/B vs Normal)	241	0.871 (0.346-2.103)	< 0.001
Fibrosis Ishak score (0/1/2/3/4/5/6 vs Normal)	215	1.497 (0.845-2.687)	< 0.001
Vascular invasion (Yes/No vs Normal)	318	1.356 (0.853-2.159)	< 0.001
OS event (Alive/Dead vs Normal)	424	1.674 (0.657-2.657)	< 0.001
OS event (Alive vs Dead)	424	1.674 (0.657-2.657)	< 0.05
PFI event (Alive/Dead vs Normal)	420	1.574 (0.457-2.357)	< 0.001
DSS event (Alive/Dead vs Normal)	380	1.474 (0.357-2.157)	< 0.001

Abbreviations: C18orf54, Chromosome 18 Open Reading Frame 54; OR, Odds Ratio; OR, Odds Ratio; OS, overall survival; PFI, Progression Free Interval; DSS, disease specific survival.

ers or immunotherapeutic targets for HCC is of great clinical importance. Our study found that the top three immunosuppressants with strong association with C18orf54 were Hepatitis A virus cellular receptor 2 (HAVCR2), T cell immunoreceptor with Ig and ITIM domains (TIGIT) and Cytotoxic T lymphocyte associate protein-4 (CTLA4). HAVCR2 alias T-cell immunoglobulin-3 (Tim-3), Tim-3 was identified 13 years ago as a CD4 T helper 1 (Th1) and CD8 T cytotoxicity 1 (Tc1) in the production of IFN-γ A cell surface molecule selectively expressed on T cells, one study demonstrated high Tim-3 expression in tumors, contributing to suppression of protective immunity [40]. TIGIT (T cell immunoglobulin and ITIM structural domain) was first identified by bioinformatics algorithms as a new member of the CD28 family, and TIGIT can suppress antitumor immunity through multiple mechanisms, including direct inhibition of effector $CD8^+$ T cell function and indirect inhibition by promoting Treg cell function [40]. CTLA-4 is a member of the immunoglobulin-associated receptor family responsible for various aspects of T cell immune regulation [41], and anti-CTLA-4 antibody treatment leads to tumor regression and relative resistance to cancer reinoculation [42]. In summary, C18orf54 shows a positive correlation with the three immune checkpoints mentioned above, which also gives us a new idea of treatment for patients with HCC, moreover, an alternative model has been proposed in which CTLA-4 and PD-1 represent the first layer of co-suppressor receptors, which are mainly responsible for maintaining self-tolerance and limiting T cell clonotypes in lymphoid organs, while Lag-3, Tim-3 and TIGIT represent the second layer of co-inhibitory molecules, which have a unique and specific role in regulating immune responses, especially at sites of tissue inflammation [40], and in our study C18orf54 showed high correlation exactly with the bilayer co-inhibitory molecules proposed in the above model, which can be studied in depth in subsequent studies to explore new hepatocellular carcinoma immunotherapeutic targets.

At the same time, we also analyzed the clinical parameters and prognosis associated with

Table 8. Clinical features and prognosis of C18orf54

Characteristic	Low expression of C18orf54	High expression of C18orf54	P (OS)	P (DSS)
n	187	187		
T stage, n (%)			0.001	0.012
T1	102 (27.5%)	81 (21.8%)		
T2	49 (13.2%)	46 (12.4%)		
T3	32 (8.6%)	48 (12.9%)		
T4	3 (0.8%)	10 (2.7%)		
Pathologic stage, n (%)			0.003	0.029
Stage I	97 (27.7%)	76 (21.7%)		
Stage II	48 (13.7%)	39 (11.1%)		
Stage III	31 (8.9%)	54 (15.4%)		
Stage IV	3 (0.9%)	2 (0.6%)		
Tumor status, n (%)			0.001	0.011
Tumor free	106 (29.9%)	96 (27%)		
With tumor	71 (20%)	82 (23.1%)		
Age, n (%)			0.001	0.01
≤60	76 (20.4%)	101 (27.1%)		
>60	111 (29.8%)	85 (22.8%)		
Residual tumor, n (%)			0.003	0.004
R0	171 (49.6%)	156 (45.2%)		
R1	4 (1.2%)	13 (3.8%)		
R2	1 (0.3%)	0 (0%)		
Histologic grade, n (%)			0.001	0.01
G1	37 (10%)	18 (4.9%)		
G2	96 (26%)	82 (22.2%)		
G3	51 (13.8%)	73 (19.8%)		
G4	2 (0.5%)	10 (2.7%)		
None	66 (27.8%)	52 (21.9%)		

Abbreviations: C18orf54, Chromosome 18 Open Reading Frame 54; OS, overall survival; DSS, disease specific survival.

C18orf54 and HCC, and found that C18orf54 was closely related to the prognostic correlates especially. C18orf54 was used to predict the survival probability of patients with HCC after 1, 2 and 3 years, showing a high agreement with the actually-observed survival probability model. The predictive value of C18orf54 for the prognosis of patients with HCC was also reinforced. Finally, by exploring C18orf54-drug interactions, we eventually located 4 drugs, cyclosporine, quercetin, testosterone and calcitriol. Cyclosporine is a steroid-preserved immunosuppressant used in organ and bone marrow transplantation and in ulcerative colitis, rheumatoid Calcitriol, the active metabolite of vitamin D, is used in the treatment of hyperparathyroidism and in dialysis patients to combat hypocalcemia. Some relevant studies have shown that Cyclosporine A and tacrolimus inhibit bladder cancer growth through downregulation of NFATc1 [43]. Quercetin is a natural flavonoid found in food and natural supplement products. Quercetin is the main representative of the flavonoid subclass of flavanols. Quercetin is ubiquitously found in fruits and vegetables and is one of the most common dietary flavanols in the Western diet. The anticancer effects of quercetin include its ability to promote loss of cell viability, apoptosis and autophagy through regulation of PI3K/Akt/mTOR, Wnt/-catenin and MAPK/ERK1/2 pathways [44]. Testosterone is a hormone used in the treatment of hypogonadism, female breast cancer or vasodilatory symptoms of menopause. Testosterone combined with anastrozole effectively treated symptoms of hormone deficiency in BCA survivors and was not associated with recurrent disease. Most notably,

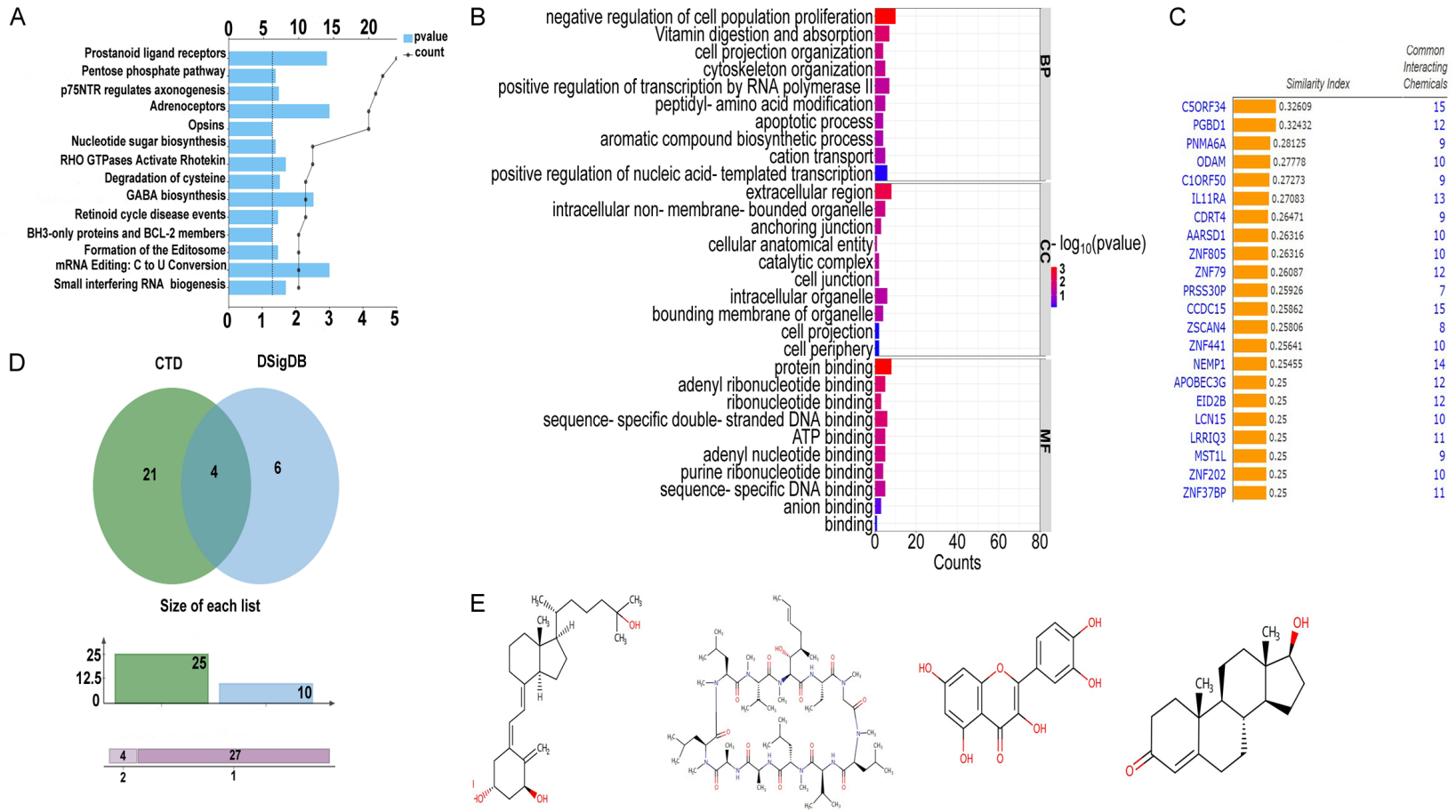

Figure 14. Potential drug targets of C18orf54 in HCC. A. KEGG enrichment pathway of C18orf54-associated drugs. B. C18orf54-associated BP, CC, MF enrichment maps. C. Drug molecules interacting with C18orf54. D. Vinci cross plots between C18orf54-related drugs obtained from 2 databases. E. Molecular formulae of Cyclosporine, Quercetin, Testosterone and Calcitriol drug structures. CTD, The Comparative Toxicogenomic Database; DsigDB, Drug Signatures Database; BP, Biologic processes; CC, Cell components; MF, Molecular functions; KEGG, Kyoto Encyclopedia of Genes and Genomes; HCC, Hepatocellular carcinoma; C18orf54, Chromosome 18 Open Reading Frame 54.

Testosterone and anastrozole implants placed in breast tissue surrounding malignant tumors significantly reduced BCA tumor size, further supporting Testosterone direct antiproliferative, protective and therapeutic effect [45]. Calcitriol is an active metabolite of vitamin D that is used to treat hyperparathyroidism and is also used in dialysis patients to combat hypocalcemia. We show that Calcitriol acts as a master transcriptional regulator of pancreatic stellate cells to reprise the quiescent state, resulting in induced stromal remodeling, increased intertumoral gemcitabine, reduced tumor volume, and a 57% increase in survival compared to chemotherapy alone [46]. All of the aforementioned drugs are effective in reducing the expression of mRNA in HCC and may provide a new idea in the clinical use or combination of drugs in patients with HCC.

Currently, our study provides a preliminary theoretical basis, while subsequent experimental and clinical validation is still needed to obtain accurate empirical evidence. Some limitations remain in our study, first of all, our findings are based on retrospective data from public databases, but more prospective data and a larger HCC cohort are needed to confirm its clinical applicability. Secondly, the role of C18orf54 in tumor immune infiltration needs further validation in vitro or in vivo. Further functional studies are needed to elucidate the aspects of signaling pathways that C18orf54 can regulate in HCC. In a word, C18orf54 is involved in the immune infiltration and promotes the poor prognosis of HCC, which could be a candidate biomarker for HCC.

Acknowledgements

This work was supported by Science and Technology Department of Xinjiang Uygur Autonomous Region, Key Laboratory Open Project (2022D04030).

Disclosure of conflict of interest

None.

Address correspondence to: Xiumin Ma, State Key Laboratory of Pathogenesis, Prevention and Treatment of High Incidence Diseases in Central Asia, Clinical Laboratory Center, Tumor Hospital Affiliated to Xinjiang Medical University, No. 393 New Road, Urumqi 830011, Xinjiang, P. R. China. E-mail: maxiumin1210@sohu.com

References

[1] Reyes-Farias M and Carrasco-Pozo C. The anticancer effect of quercetin: molecular implications in cancer metabolism. Int J Mol Sci 2019; 20: 3177.

[2] Yang M, Parikh ND, Liu H, Wu E, Rao H, Feng B, Lin A, Wei L and Lok AS. Incidence and risk factors of hepatocellular carcinoma in patients with hepatitis C in China and the United States. Sci Rep 2020; 10: 20922.

[3] Reinders MTM, van Meer S, Burgmans MC, de Jong KP, Klumpen HJ, de Man RA, Ramsoekh DS, Sprengers D, Tjwa ETTL, de Vos-Geelen J, van Erpecum KJ and van der Geest LGM; Dutch Hepatocellular & Cholangiocarcinoma Group (DHCG). Trends in incidence, diagnosis, treatment and survival of hepatocellular carcinoma in a low-incidence country: data from the Netherlands in the period 2009-2016. Eur J Cancer 2020; 137: 214-223.

[4] Petrick JL, Florio AA, Znaor A, Ruggieri D, Laversanne M, Alvarez CS, Ferlay J, Valery PC, Bray F and McGlynn KA. International trends in hepatocellular carcinoma incidence, 1978-2012. Int J Cancer 2020; 147: 317-330.

[5] Anwanwan D, Singh SK, Singh S, Saikam V and Singh R. Challenges in liver cancer and possible treatment approaches. Biochim Biophys Acta Rev Cancer 2020; 1873: 188314.

[6] Demir T, Lee SS and Kaseb AO. Systemic therapy of liver cancer. Adv Cancer Res 2021; 149: 257-294.

[7] Wang T, Xu L, Jia R and Wei J. MiR-218 suppresses the metastasis and EMT of HCC cells via targeting SERBP1. Acta Biochim Biophys Sin (Shanghai) 2017; 49: 383-391.

[8] Villanueva A. Hepatocellular carcinoma. N Engl J Med 2019; 380: 1450-1462.

[9] Cornelison R, Llaneza DC and Landen CN. Emerging therapeutics to overcome chemoresistance in epithelial ovarian cancer: a mini-review. Int J Mol Sci 2017; 18: 2171.

[10] Tsuchiya N, Sawada Y, Endo I, Saito K, Uemura Y and Nakatsura T. Biomarkers for the early diagnosis of hepatocellular carcinoma. World J Gastroenterol 2015; 21: 10573-10583.

[11] Wang W and Wei C. Advances in the early diagnosis of hepatocellular carcinoma. Genes Dis 2020; 7: 308-319.

[12] Fox R, Berhane S, Teng M, Cox T, Tada T, Toyoda H, Kumada T, Kagebayashi C, Satomura S and Johnson PJ. Biomarker-based prognosis in hepatocellular carcinoma: validation and extension of the BALAD model. Br J Cancer 2014; 110: 2090-2098.

[13] Abe T, Tashiro H, Kobayashi T, Hattori M, Kuroda S and Ohdan H. Glasgow prognostic score and prognosis after hepatectomy for he-

patocellular carcinoma. World J Surg 2017; 41: 1860-1870.
[14] Liu H, Gao Y, Hu S, Fan Z, Wang X and Li S. Bioinformatics analysis of differentially expressed rhythm genes in liver hepatocellular carcinoma. Front Genet 2021; 12: 680528.
[15] Zhang Q, Xiao Z, Sun S, Wang K, Qian J, Cui Z, Tao T and Zhou J. Integrated proteomics and bioinformatics to identify potential prognostic biomarkers in hepatocellular carcinoma. Cancer Manag Res 2021; 13: 2307-2317.
[16] Zhang P, Feng J, Wu X, Chu W, Zhang Y and Li P. Bioinformatics analysis of candidate genes and pathways related to hepatocellular carcinoma in China: a study based on public databases. Pathol Oncol Res 2021; 27: 588532.
[17] Liao Y, Yuan S, Chen X, Zhu P, Li J, Qin L and Liao W. Up-regulation of BRCA1-associated RING domain 1 promotes hepatocellular carcinoma progression by targeting Akt signaling. Sci Rep 2017; 7: 7649.
[18] Zhu X, Wang Z, Qiu X, Wang W, Bei C, Tan C, Qin L, Ren Y and Tan S. Rs2303428 of MSH2 is associated with hepatocellular carcinoma prognosis in a Chinese population. DNA Cell Biol 2018; 37: 634-641.
[19] Hu H, Zhong T and Jiang S. H2AFX might be a prognostic biomarker for hepatocellular carcinoma. Cancer Rep (Hoboken) 2023; 6: e1684.
[20] Dong M, Chen J, Deng Y, Zhang D, Dong L and Sun D. H2AFZ is a prognostic biomarker correlated to TP53 mutation and immune infiltration in hepatocellular carcinoma. Front Oncol 2021; 11: 701736.
[21] Szklarczyk D, Gable AL, Lyon D, Junge A, Wyder S, Huerta-Cepas J, Simonovic M, Doncheva NT, Morris JH, Bork P, Jensen LJ and Mering CV. STRING v11: protein-protein association networks with increased coverage, supporting functional discovery in genome-wide experimental datasets. Nucleic Acids Res 2019; 47: D607-D613.
[22] Wang H, Huo X, Yang XR, He J, Cheng L, Wang N, Deng X, Jin H, Wang N, Wang C, Zhao F, Fang J, Yao M, Fan J and Qin W. STAT3-mediated upregulation of lncRNA HOXD-AS1 as a ceRNA facilitates liver cancer metastasis by regulating SOX4. Mol Cancer 2017; 16: 136.
[23] Schulze K, Imbeaud S, Letouze E, Alexandrov LB, Calderaro J, Rebouissou S, Couchy G, Meiller C, Shinde J, Soysouvanh F, Calatayud AL, Pinyol R, Pelletier L, Balabaud C, Laurent A, Blanc JF, Mazzaferro V, Calvo F, Villanueva A, Nault JC, Bioulac-Sage P, Stratton MR, Llovet JM and Zucman-Rossi J. Exome sequencing of hepatocellular carcinomas identifies new mutational signatures and potential therapeutic targets. Nat Genet 2015; 47: 505-511.
[24] Li T, Fu J, Zeng Z, Cohen D, Li J, Chen Q, Li B and Liu XS. TIMER2.0 for analysis of tumor-infiltrating immune cells. Nucleic Acids Res 2020; 48: W509-W514.
[25] Baylin SB and Herman JG. DNA hypermethylation in tumorigenesis: epigenetics joins genetics. Trends Genet 2000; 16: 168-174.
[26] Liu T, Wu H, Qi J, Qin C and Zhu Q. Seven immune-related genes prognostic power and correlation with tumor-infiltrating immune cells in hepatocellular carcinoma. Cancer Med 2020; 9: 7440-7452.
[27] He H, Wu J, Zang M, Wang W, Chang X, Chen X, Wang R, Wu Z, Wang L, Wang D, Lu F, Sun Z and Qu C. CCR6(+) B lymphocytes responding to tumor cell-derived CCL20 support hepatocellular carcinoma progression via enhancing angiogenesis. Am J Cancer Res 2017; 7: 1151-1163.
[28] Geh D, Leslie J, Rumney R, Reeves HL, Bird TG and Mann DA. Neutrophils as potential therapeutic targets in hepatocellular carcinoma. Nat Rev Gastroenterol Hepatol 2022; 19: 257-273.
[29] Palucka K and Banchereau J. Cancer immunotherapy via dendritic cells. Nat Rev Cancer 2012; 12: 265-277.
[30] Noda T, Shimoda M, Ortiz V, Sirica AE and Wands JR. Immunization with aspartate-beta-hydroxylase-loaded dendritic cells produces antitumor effects in a rat model of intrahepatic cholangiocarcinoma. Hepatology 2012; 55: 86-97.
[31] Freitas-Lopes MA, Mafra K, David BA, Carvalho-Gontijo R and Menezes GB. Differential location and distribution of hepatic immune cells. Cells 2017; 6: 48.
[32] Fukushige S and Horii A. DNA methylation in cancer: a gene silencing mechanism and the clinical potential of its biomarkers. Tohoku J Exp Med 2013; 229: 173-185.
[33] Mantovani A, Allavena P, Sica A and Balkwill F. Cancer-related inflammation. Nature 2008; 454: 436-444.
[34] Shapouri-Moghaddam A, Mohammadian S, Vazini H, Taghadosi M, Esmaeili SA, Mardani F, Seifi B, Mohammadi A, Afshari JT and Sahebkar A. Macrophage plasticity, polarization, and function in health and disease. J Cell Physiol 2018; 233: 6425-6440.
[35] Singh S, Hassan D, Aldawsari HM, Molugulu N, Shukla R and Kesharwani P. Immune checkpoint inhibitors: a promising anticancer therapy. Drug Discov Today 2020; 25: 223-229.
[36] Jiao Y, Yi M, Xu L, Chu Q, Yan Y, Luo S and Wu K. CD38: targeted therapy in multiple myeloma and therapeutic potential for solid cancers. Expert Opin Investig Drugs 2020; 29: 1295-1308.

[37] Wang S, Sun C, Li J, Zhang E, Ma Z, Xu W, Li H, Qiu M, Xu Y, Xia W, Xu L and Yin R. Roles of RNA methylation by means of N6-methyladenosine (m6A) in human cancers. Cancer Lett 2017; 408: 112-120.
[38] Anderson AC, Joller N and Kuchroo VK. Lag-3, Tim-3, and TIGIT: co-inhibitory receptors with specialized functions in immune regulation. Immunity 2016; 44: 989-1004.
[39] Rowshanravan B, Halliday N and Sansom DM. CTLA-4: a moving target in immunotherapy. Blood 2018; 131: 58-67.
[40] Leach DR, Krummel MF and Allison JP. Enhancement of antitumor immunity by CTLA-4 blockade. Science 1996; 271: 1734-1736.
[41] Lesterhuis WJ, Salmons J, Nowak AK, Rozali EN, Khong A, Dick IM, Harken JA, Robinson BW and Lake RA. Synergistic effect of CTLA-4 blockade and cancer chemotherapy in the induction of anti-tumor immunity. PLos One 2013; 8: e61895.
[42] Du X, Tang F, Liu M, Su J, Zhang Y, Wu W, Devenport M, Lazarski CA, Zhang P, Wang X, Ye P, Wang C, Hwang E, Zhu T, Xu T, Zheng P and Liu Y. A reappraisal of CTLA-4 checkpoint blockade in cancer immunotherapy. Cell Res 2018; 28: 416-432.
[43] Kawahara T, Kashiwagi E, Ide H, Li Y, Zheng Y, Miyamoto Y, Netto GJ, Ishiguro H and Miyamoto H. Cyclosporine A and tacrolimus inhibit bladder cancer growth through down-regulation of NFATc1. Oncotarget 2015; 6: 1582-93.
[44] Dajas F. Life or death: neuroprotective and anticancer effects of quercetin. J Ethnopharmacol 2012; 143: 383-396.
[45] Glaser R and Dimitrakakis C. Testosterone and breast cancer prevention. Maturitas 2015; 82: 291-295.
[46] Sherman MH, Yu RT, Engle DD, Ding N, Atkins AR, Tiriac H, Collisson EA, Connor F, Van Dyke T, Kozlov S, Martin P, Tseng TW, Dawson DW, Donahue TR, Masamune A, Shimosegawa T, Apte MV, Wilson JS, Ng B, Lau SL, Gunton JE, Wahl GM, Hunter T, Drebin JA, O'Dwyer PJ, Liddle C, Tuveson DA, Downes M and Evans RM. Vitamin D receptor-mediated stromal reprogramming suppresses pancreatitis and enhances pancreatic cancer therapy. Cell 2014; 159: 80-93.

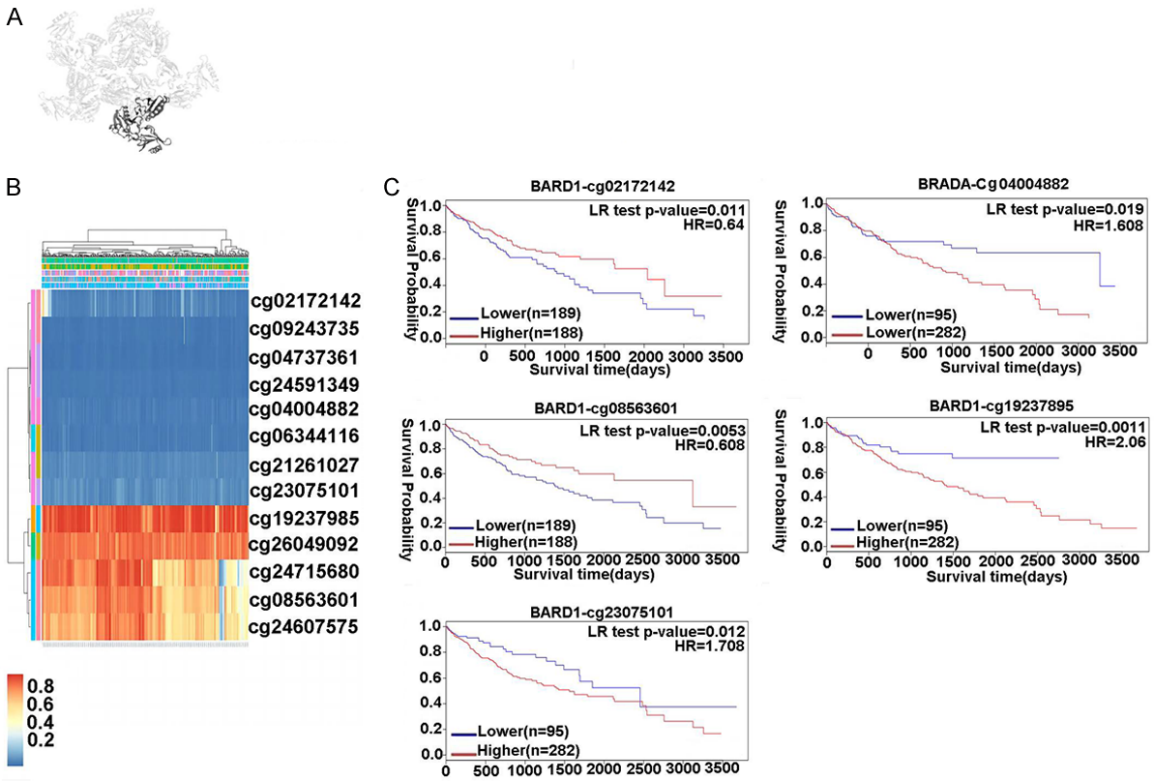

Supplementary Figure 1. Methylation mutation sites of BARD1 in HCC. A. 3D structure of C18orf54. B, C. CpG clustering analysis of the BARD1 heat map and methylation levels associated with patient characteristics and gene subregions. LR, likelihood ratio; HR, Hazard Ratio; C18orf54, Chromosome 18 Open Reading Frame 54.

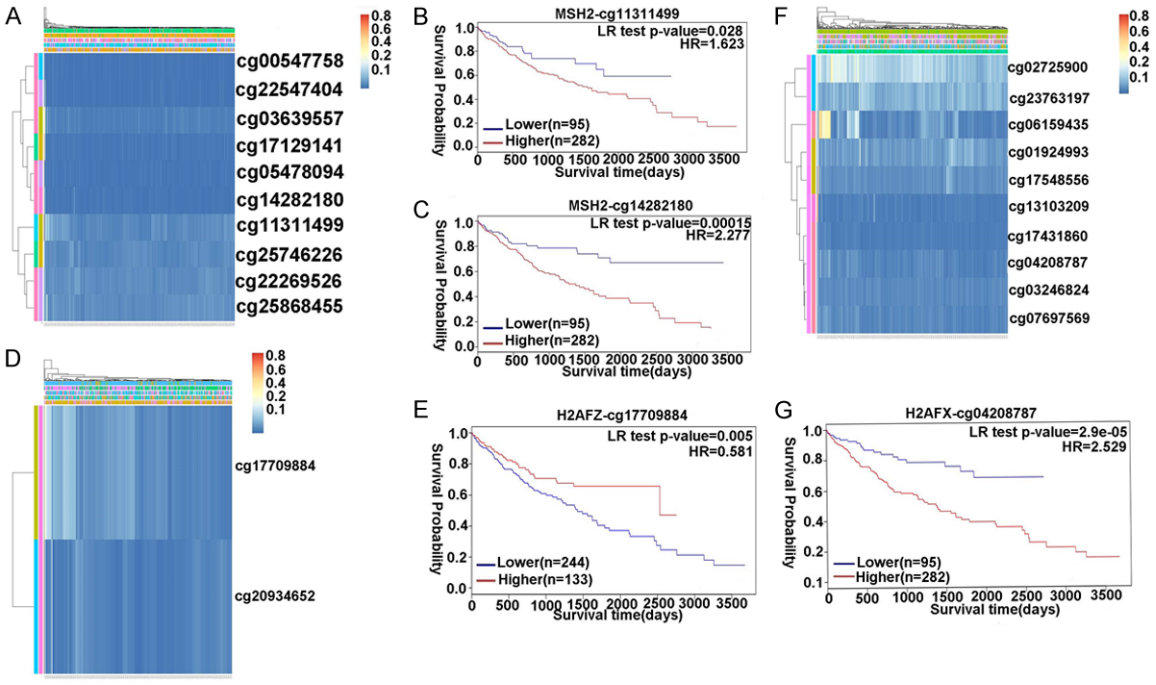

Supplementary Figure 2. Methylation mutation sites of MSH2, H2AFZ and H2AFX in HCC. A-C. CpG clustering analysis of MSH2 heat map and methylation levels associated with patient characteristics and gene subregions. D, E. CpG clustering analysis of the H2AFZ heat map and methylation levels associated with patient characteristics and gene subregions. F, G. CpG clustering analysis of H2AFX heat map and methylation levels associated with patient characteristics and gene subregions. LR, likelihood ratio; HR, Hazard Ratio; C18orf54, Chromosome 18 Open Reading Frame 54.

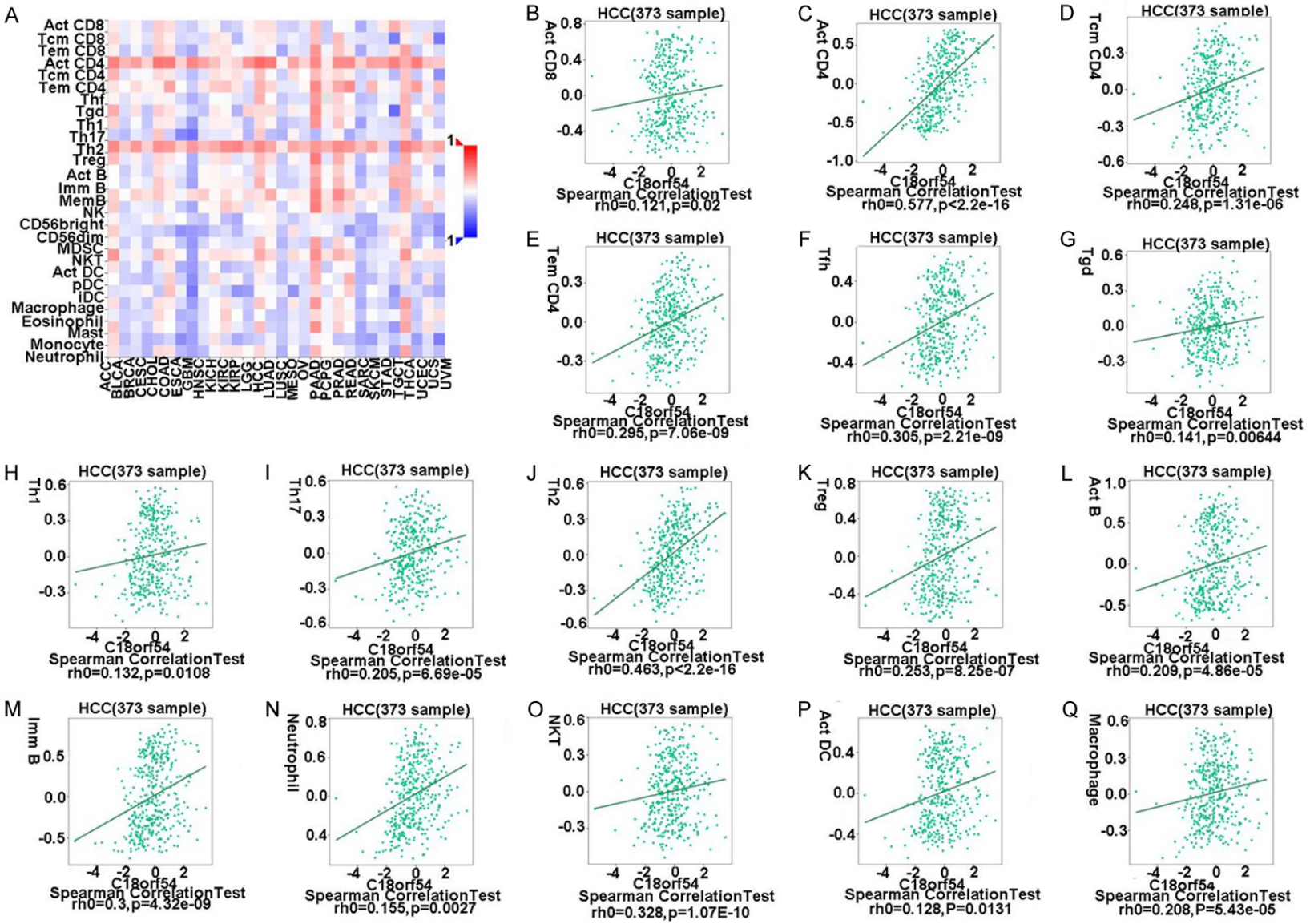

Supplementary Figure 3. Correlation of C18orf54 with immune cells. A. Heat map of the correlation between C18orf54 and immune cells in pan-cancer. B-Q. Relationship between C18orf54 and various immune cells in HCC. HCC, hepatocellular carcinoma; C18orf54, Chromosome 18 Open Reading Frame 54; rh0, regression coefficient.

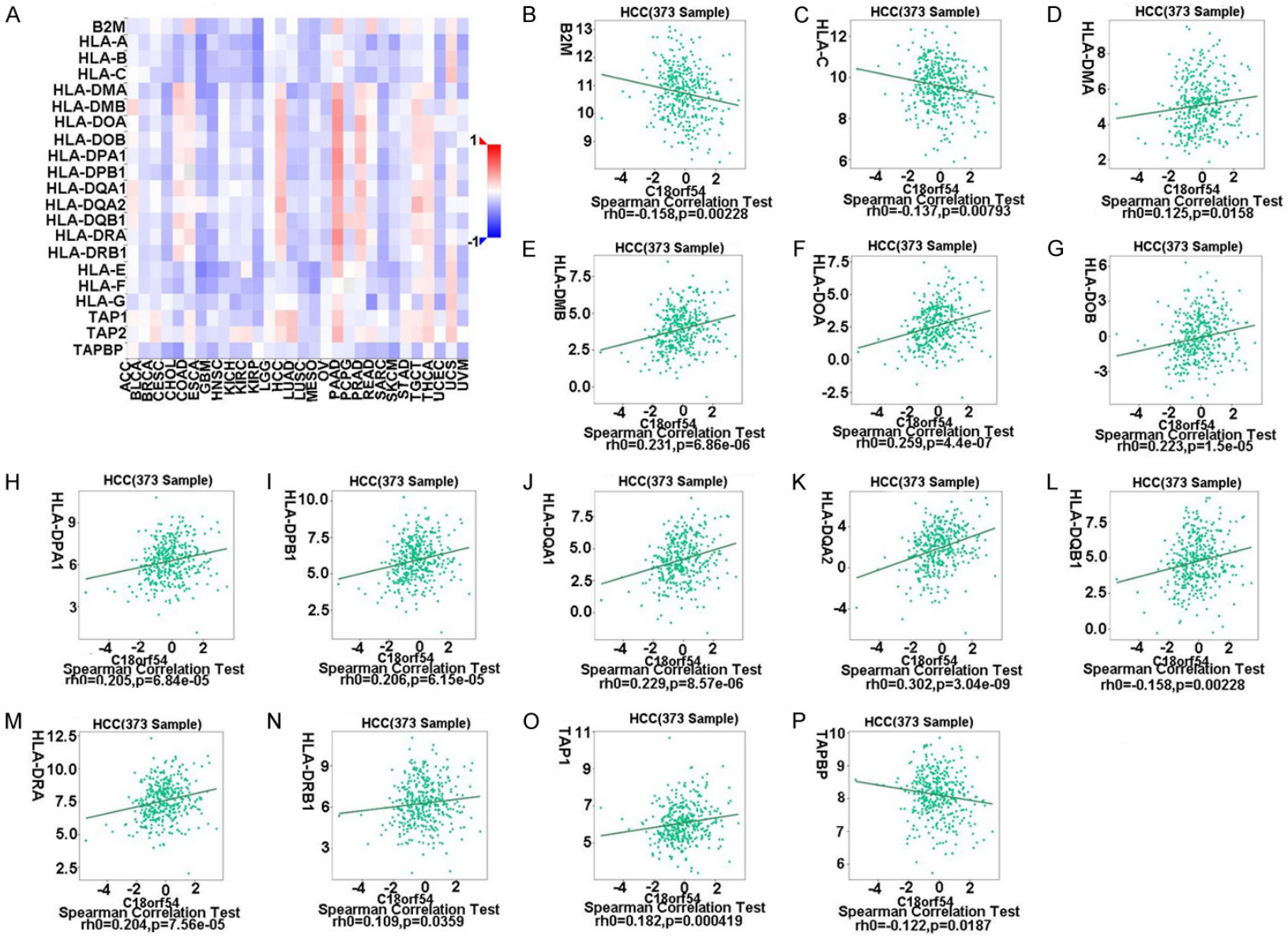

Supplementary Figure 4. Correlation between C18orf54 and immune checkpoints (immunostimulants) in HCC. A. Heat map of the correlation between C18orf54 and immunostimulatory sites in pan-cancer. B-P. Relationship between C18orf54 in HCC and each immunostimulatory site. HCC, hepatocellular carcinoma; C18orf54, Chromosome 18 Open Reading Frame 54; rh0, regression coefficient.

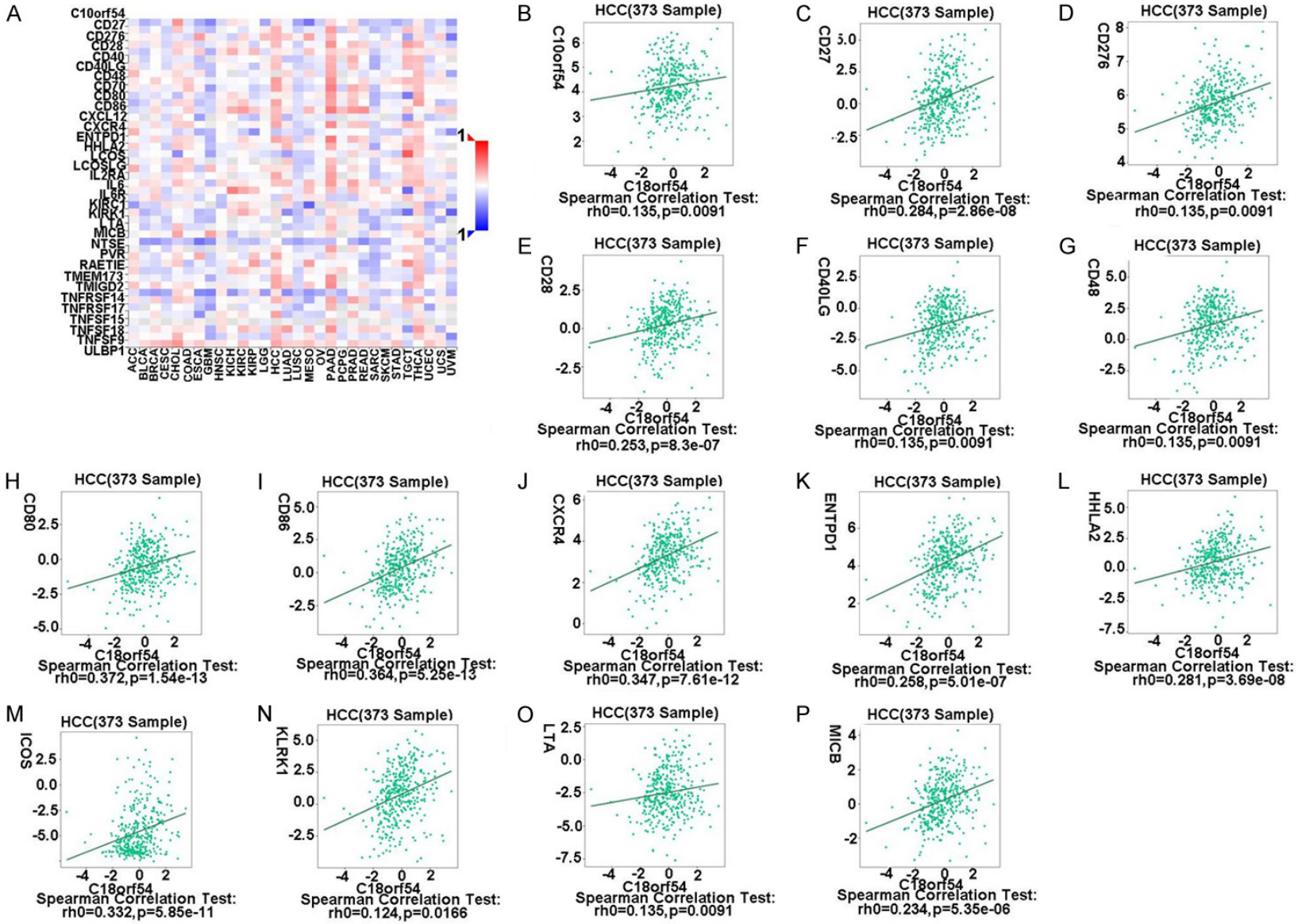

Supplementary Figure 5. Correlation between C18orf54 and MHC I/II in HCC. A. Heat map of the correlation between C18orf54 and MHC I/II sites in pan-cancer. B-P. Relationship between C18orf54 in HCC and each MHC I/II site. HCC, hepatocellular carcinoma; C18orf54, Chromosome 18 Open Reading Frame 54; rh0, regression coefficient.

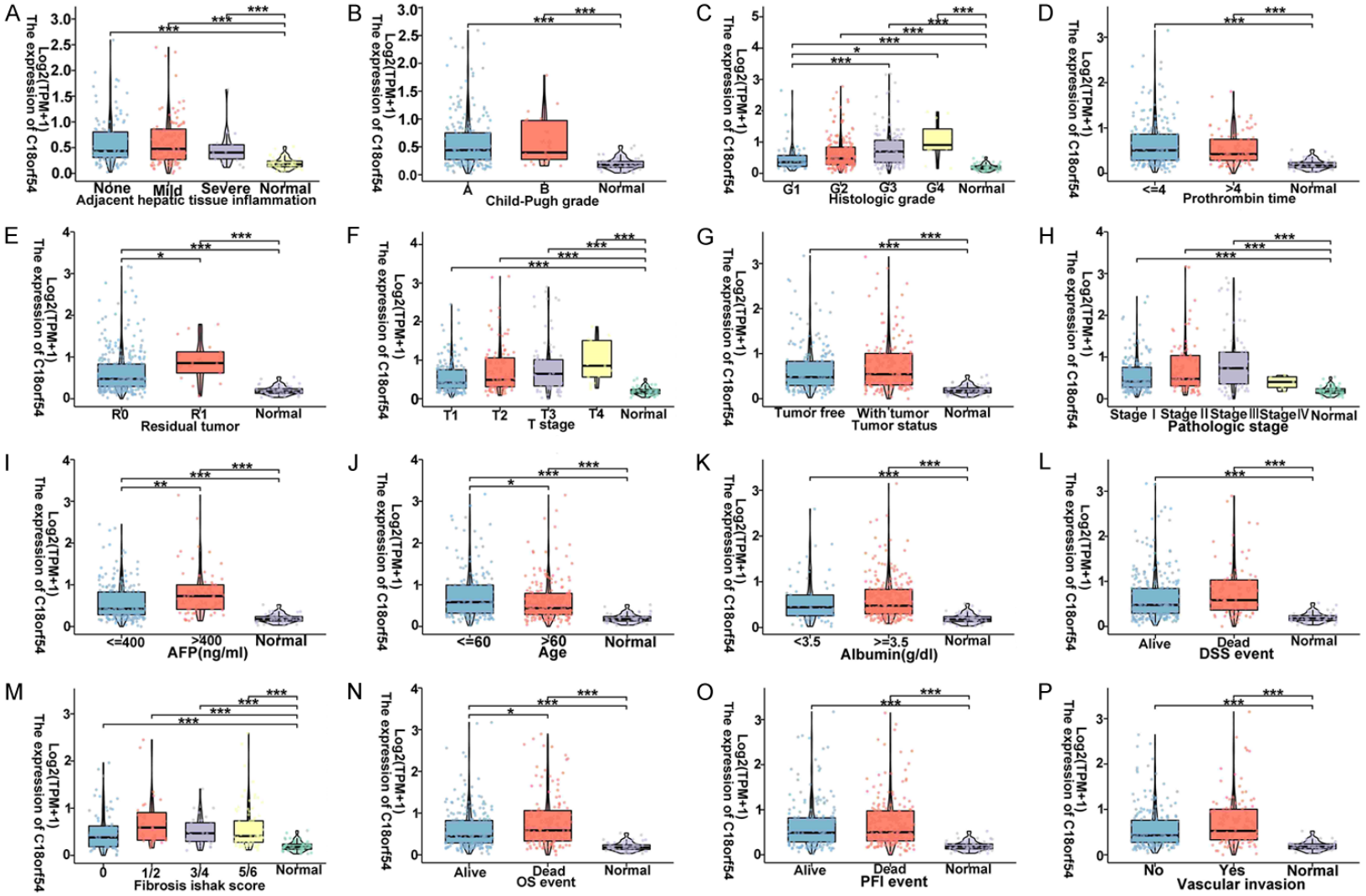

Supplementary Figure 6. High expression of C18orf54 is associated with worse prognosis. A-P. C18orf54 and Prothrombin time, Adjacent hepatic tissue inflammation, Pathologic stage, Tumor status, T stage, Residual tumor, Histologic grade child-Pugh grade, Fibrosis Ishak score, Vascular invasion, OS event, DSS event, PFI event correlation of clinical indicators. *P < 0.05, **P < 0.01, ***P < 0.001. C18orf54, Chromosome 18 Open Reading Frame 54.

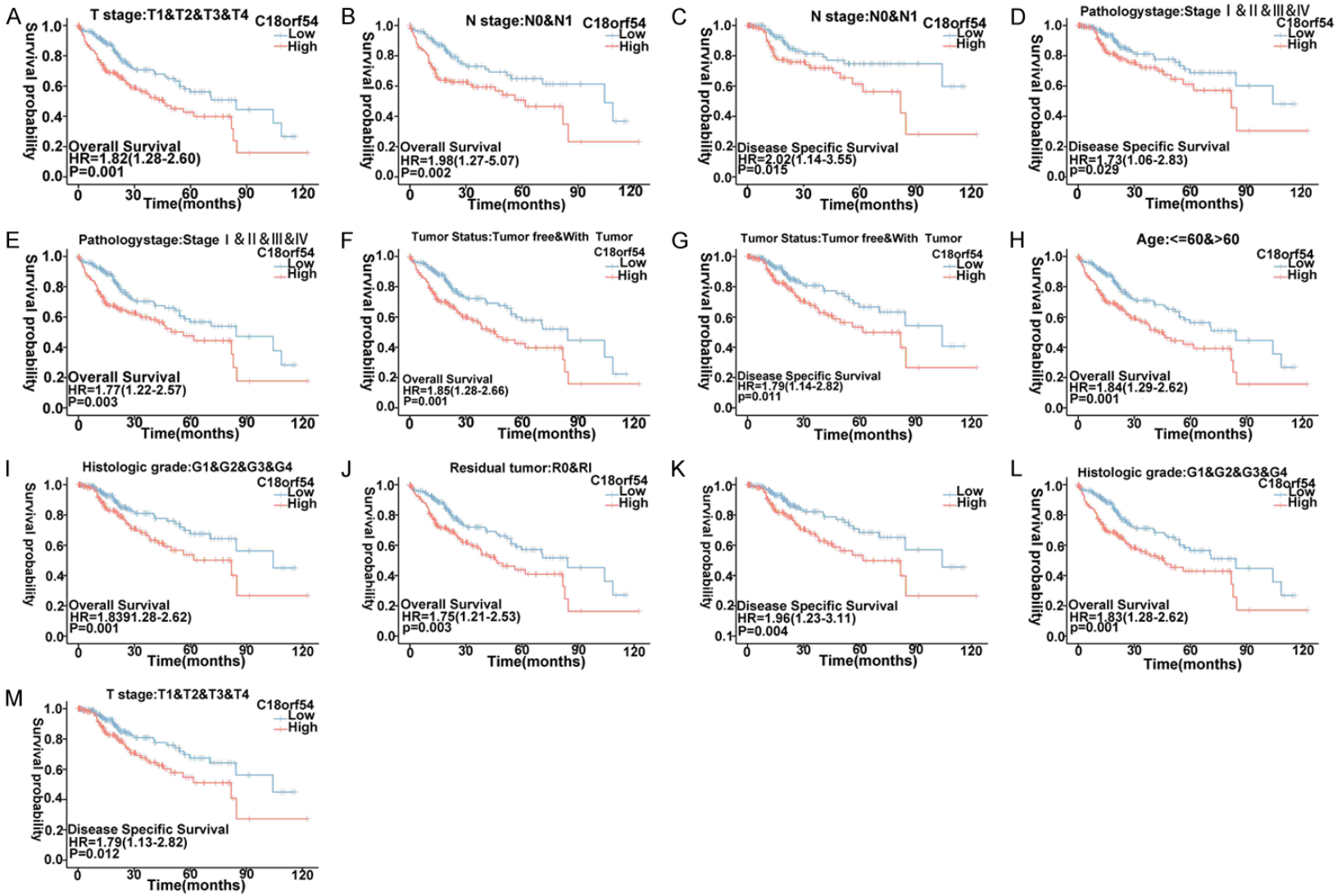

Supplementary Figure 7. High expression of C18orf54 is associated with worse survival. A-M. C18orf54 and Pathologic stage, Tumor status, T stage, Residual tumor, Histologic grade, age, N stage, OS event, DSS event correlation of clinical indicators. C18orf54, Chromosome 18 Open Reading Frame 54; OS, overall survival; DSS, disease specific survival.